ATLAS NOTE

ATL-PHYS-PUB-2015-007

25th March 2015

A study of the sensitivity to the Pythia8 parton shower parameters of $t\bar{t}$ production measurements in pp collisions at $\sqrt{s}$ = 7 TeV with the ATLAS experiment at the LHC

The ATLAS Collaboration

Abstract

Various measurements of $t\bar{t}$ observables, performed by the ATLAS experiment in pp collisions at $\sqrt{s}$ = 7 TeV, are used to constrain the initial- and final-state radiation parameters of the Pythia8 Monte Carlo generator. The resulting tunes are compared to previous tunes to the Z boson transverse momentum at the LHC, and to the LEP event shapes in Z boson hadronic decays. Such a comparison provides a test of the universality of the parton shower model. The tune of Pythia8 to the $t\bar{t}$ measurements is applied to the next-to-leading-order generators MadGraph5_aMC@NLO and Powheg, and additional parameters of these generators are tuned to the $t\bar{t}$ data. For the first time in the context of parton shower tuning in Monte Carlo simulations, the correlation of the experimental uncertainties has been used to constrain the parameters of the Monte Carlo models.

ATL-PHYS-PUB-2015-007
25 March 2015

1 Introduction

The physics models employed in the Monte Carlo (MC) event generators are expected to describe simultaneously a large variety of hard scattering processes in different types of collisions [1]. Stringent tests of the universality of such models can be obtained by performing independent optimisation of their parameters, henceforth referred to as *tunes*, on various hard scattering processes, on various observables, at various collider energies, or with different collider types [2]. As suggested in Ref. [3], the consistency of independent tunes supports the universality of the model, whereas deviations from this universal behaviour can be associated with a breakdown of the modelling. The observed deviations between data and predictions, and the tensions between the various observables, can provide important information on the nature of the breakdown.

Measurements of $t\bar{t}$ production in hadronic collisions are sensitive to the parameters of the parton shower models. At the LHC pp collider, for the first time, $t\bar{t}$ processes can be measured with enough accuracy to be used for constraining the parameters of the MC models. The ATLAS experiment has performed various measurements of $t\bar{t}$ observables in pp collisions at $\sqrt{s} = 7$ TeV, sensitive to QCD radiation [4–7], some of which have been recently used in the A14 [8] global tune of Pythia8 [9]. This note aims at studying the sensitivity of these $t\bar{t}$ measurements to the initial- (ISR) and final-state radiation (FSR) parameters of the Pythia8 MC. Also, by performing independent tunes to these measurements, the resulting optimised values of the parameters can be compared to the values constrained by other observables, such as the Z boson transverse momentum, p_{T}, as measured by ATLAS [10] and event shapes in Z boson hadronic decay as measured at LEP [11–14]. The compatibility of the resulting parameters is a prerequisite for the use of the $t\bar{t}$ measurements in the context of global tunes.

The modelling of ISR and FSR in $t\bar{t}$ events is crucial for a precise measurement of the mass of the top quark, m_t. In the most precise single measurement of m_t at the Tevatron, performed with the D0 experiment [15, 16], the uncertainty due to the modelling of ISR and FSR is constrained from the measurement of the Z/γ^* boson transverse momentum distribution [17], an idea first introduced by the CDF experiment in Ref. [18]. This technique, which provides a significant reduction of the modelling uncertainty, assumes the universality of the parton shower model between Z boson and $t\bar{t}$ production. Whereas at the Tevatron proton-antiproton collider both processes are dominated by quark-antiquark initiated production, at the LHC the $t\bar{t}$ process is dominated by gluon-gluon initiated production, and even more so the universality of ISR needs to be verified.

The NLO+PS MC event generators include next-to-leading-order (NLO) corrections, in the perturbative expansion in the strong-coupling constant α_s, to the calculations of the matrix elements of the $pp \to t\bar{t}$ process, and supplement them with parton showers (PS). With respect to Pythia8, which calculates the hard scattering only at leading-order (LO), the NLO+PS predictions are less sensitive to variations of the renormalisation and factorisation scales and have better accuracy in the total cross sections rates. The NLO+PS generators are also expected to benefit from an improved tune of the parton showers, and to this purpose, the Pythia8 tunes to the ATLAS $t\bar{t}$ measurements are applied to the NLO+PS generators Powheg+Pythia8 [19–21] and MadGraph5_aMC@NLO+Pythia8 [22]. Additional parameters of the Powheg and MadGraph5_aMC@NLO generators, which show sensitivity to the $t\bar{t}$ measurements, are tuned to the data.

This note is organised as follows: Section 2 describes the data sets used, the parameters of models, and the methodology of the parameter optimisation. Section 3 shows the sensitivity of the $t\bar{t}$ measurements to the

MC parameter variations. Sections 4 and 5 present tunes of the parameters governing ISR and FSR, respectively. Section 6 presents a simultaneous tune of the ISR and FSR parameters. Sections 7 and 8 show the application of the Pythia8 tune to the $t\bar{t}$ data to the NLO+PS generators MadGraph5_aMC@NLO and Powheg. Section 9 summarises the results.

2 Methodology

Three ATLAS measurements at $\sqrt{s} = 7$ TeV are used to constrain the ISR and FSR parameters of the Pythia8 MC: differential $t\bar{t}$ cross sections as functions of jet multiplicity and jet transverse momentum [6], $t\bar{t}$ production with a veto on additional central jet activity [4], henceforth referred to as gap-fraction measurements, and jet shapes in $t\bar{t}$ events [5]. The statistical correlations among the various observables of these $t\bar{t}$ measurements were not studied, hence a set of observables is chosen, which are sufficiently statistically independent, so as to avoid any bias in the results. In Ref. [6] the $t\bar{t}$ production cross-section is measured differentially in jet multiplicity and in jet transverse momentum in the single-lepton channel, without explicit separation between jets related to $t\bar{t}$ decays and additional jets. The jet multiplicity is measured for several different jet transverse momentum thresholds and the cross section with respect to the jet p_{T} is measured separately for the five highest p_{T} jets. The differential cross sections as functions of the leading-jet p_{T}, of the 5th leading-jet p_{T}, of jet multiplicity for jets with $p_{\mathrm{T}} \geqslant 25$ GeV and jet multiplicity for jets with $p_{\mathrm{T}} \geqslant 80$ GeV are used. The overall normalisation of these observables is sensitive to higher-order QCD corrections. In order to reduce the effect of missing higher-order QCD corrections on the minimisation of the MC parameters, the predictions of the $t\bar{t}$ + jets differential cross sections are normalised to the data, separately for each observable. From Ref. [4], only the inclusive gap fraction as a function of the leading-jet p_{T} threshold, Q_0, is used. This measurement is performed in the dileptonic channel, to ensure that the additional jets can easily be distinguished from the $t\bar{t}$ decay products. The gap fraction is defined as $f(Q_0) = n(Q_0)/N$ where N is the number of selected $t\bar{t}$ events and $n(Q_0)$ the fraction of those events that do not contain an additional jet with $p_{\mathrm{T}} > Q_0$ in a central rapidity interval. The inclusive gap fraction as a function of the scalar transverse momentum sum of the additional jets, Q_{sum}, is considered statistically correlated to the inclusive gap fraction as a function of Q_0, and is not used. Differential gap-fraction measurements as a function of rapidity were also measured in Ref. [4], but they are not used in this study, since the parameters of the model do not show sensitivity to the rapidity dependence of the gap fraction. In Ref. [5], the differential and integral jet shapes as a function of the jet radius r are measured for light- and b-jets in five exclusive p_{T} ranges of the jet. Samples of top-quark pair events are selected in both the single-lepton and dilepton final states. The shapes of the jets initiated by bottom-quarks from the top-quark decays are compared with those of the jets originated by light-quarks from the hadronic W boson decays in the single-lepton channel. Jet shapes are sensitive to the details of the parton-to-jet fragmentation processes, such as the value of α_S used in the branchings of FSR, the fragmentation model and the underlying event. In this study only the differential jet shapes are used. They are defined as the average fraction of transverse momentum contained within an annulus of inner radius $r_a = r - \delta r/2$ and outer radius $r_b = r + \delta r/2$, where r is measured relative to the jet axis and lies in the range $\delta r/2 \leqslant r \leqslant R - \delta r/2$.

$$\rho(r) = \frac{1}{\delta r} \cdot \frac{1}{N_{\mathrm{jets}}} \cdot \sum_{\mathrm{jets}} \frac{p_{\mathrm{T}}(r_a, r_b)}{p_{\mathrm{T}}(0, R)} \tag{1}$$

R represents the maximum radius, and is set to 0.4, the radius used in the jet reconstruction algorithm. $\delta r = 0.04$ is the width of the annulus and $p_{\mathrm{T}}(r_a, r_b)$ is the scalar sum of the p_{T} of the jet constituents

with radii between r_a and r_b. Recently, another measurement of $t\bar{t}$ production in pp collisions has been performed with the ATLAS detector [7], in which differential cross sections are presented in terms of kinematic variables whose dependence on theoretical models is minimal. This measurement, which is not included in this study, is also expected to be sensitive to QCD radiation.

The Pythia8 MC version 8.201 is used throughout this study. The 4C [23] tune with the CTEQ6L1 PDF set [24], or the more recent Monash [2] tune with the NNPDF2.3 LO PDF set [25] are used as baselines for the parameter optimisation, henceforth referred to as *tuning*. In the Pythia8 MC event generator, the matrix elements for $t\bar{t}$ production are computed at LO, and supplemented with parton showers. The $t\bar{t}$ process receives significant corrections at NLO in α_s, and such corrections need to be accounted for when performing a tuning of the parton shower parameters to observables in the $t\bar{t}$ final state. In Ref. [26] it was shown that a modification of the parton shower emission probability with a damping factor can be used to approximate the effect of NLO corrections to the $t\bar{t}$ production. The ISR emission probability $\mathcal{P}_{\text{ISR}}$ is modified as

$$\frac{\mathrm{d}\mathcal{P}_{\text{ISR}}}{\mathrm{d}p_{\text{T}}^2} \propto \frac{1}{p_{\text{T}}^2} \frac{k^2 M^2}{k^2 M^2 + p_{\text{T}}^2} \tag{2}$$

where p_{T} is the transverse momentum evolution variable, as defined in Ref. [27], M is the factorisation scale, which is set to the smaller of the squared transverse masses of the two outgoing particles, and k is a fudge factor of order unity, which corresponds to the tunable parameter $p_{\text{T,damp}}^{\text{ISR}}$. The scale $k \cdot M$ corresponds to a transition from the $1/p_{\text{T}}^2$ to the $1/p_{\text{T}}^4$ behaviour in the probability of ISR emission.

Four parameters of the Pythia8 parton shower model are studied and tuned to the data: two ISR parameters correspond to the value of the strong-coupling constant at the mass of the Z boson for ISR, $\alpha_s^{\text{ISR}}(m_Z)$, and the fudge factor for the damping of the ISR radiation, $p_{\text{T,damp}}^{\text{ISR}}$, and two FSR parameters are the value of $\alpha_s^{\text{FSR}}(m_Z)$ and the infrared cut-off $p_{\text{T,min}}^{\text{FSR}}$. A similar fudge factor for the damping of the FSR radiation, $p_{\text{T,damp}}^{\text{FSR}}$, has been considered, but the data does not show sensitivity to this parameter. Higher-order corrections can be partially absorbed in the effective values of $\alpha_s^{\text{ISR}}(m_Z)$ and $\alpha_s^{\text{FSR}}(m_Z)$. However the structure of higher-order splitting kernels differs between ISR and FSR [9], hence the $\alpha_s^{\text{ISR}}(m_Z)$ and $\alpha_s^{\text{FSR}}(m_Z)$ parameters are allowed to assume different values in the tuning. The strategy followed in this study is to first perform independent tuning of the ISR and FSR parameters: the results of these tunes can be compared to previous tunes to test the universality of the model separately for ISR and FSR. Later, a simultaneous tune of ISR and FSR is performed, which accounts for the interplay between the ISR and FSR parameters. Whereas the values of $\alpha_s^{\text{ISR}}(m_Z)$, $\alpha_s^{\text{FSR}}(m_Z)$, and $p_{\text{T,min}}^{\text{FSR}}$ are expected to be process-independent parameters of the Pythia8 parton shower model, the value of $p_{\text{T,damp}}^{\text{ISR}}$ is expected to be process-specific. Moreover, the damping of the ISR emission probability should be used only when showering LO $t\bar{t}$ matrix-element calculations, and disabled by setting `SpaceShower:pTdampMatch=0` when Pythia8 is interfaced to NLO $t\bar{t}$ or multi-leg $t\bar{t}$+jets MC generators.

After tuning the ISR and FSR parameters to the $t\bar{t}$ data, the resulting Pythia8 tune is used with the NLO+PS generators Powheg v2-r2915 [19–21, 28] and MadGraph5_aMC@NLO v2.2.2 [22]. The CT10nlo PDF set [29] is used in both Powheg and MadGraph5_aMC@NLO. The renormalisation and factorisation scales in MadGraph5_aMC@NLO are set to the sum of the transverse masses of the top and the antitop. In Powheg they are set at the generator default value Q, defined as $Q = \sqrt{m_t^2 + p_{\text{T}}^2}$, where m_t and p_{T} are the top quark mass and the top quark transverse momentum evaluated for the underlying Born configuration (i.e. before radiation). In the Powheg generator, it is possible to introduce a damping factor

Table 1: Parameter ranges used for the tuning of Pythia8, and the corresponding parameters of the 4C and Monash tunes. The '-' symbol is used in case the setting is not applicable.

Parameter	Pythia8 setting	Variation range	4C	Monash
$\alpha_s^{\mathrm{ISR}}(m_Z)$	`SpaceShower:alphaSvalue`	0.110 – 0.140	0.137	0.1365
ISR damping	`SpaceShower:pTdampMatch`	1 (fixed)	0	0
$p_{\mathrm{T,damp}}^{\mathrm{ISR}}$	`SpaceShower:pTdampFudge`	0.8 – 1.8	-	-
$\alpha_s^{\mathrm{FSR}}(m_Z)$	`TimeShower:alphaSvalue`	0.110 – 0.150	0.1383	0.1365
$p_{\mathrm{T,min}}^{\mathrm{FSR}}$ [GeV]	`TimeShower:pTmin`	0.1 – 2.0	0.4	0.5

$$F = \frac{\texttt{hdamp}^2}{p_{\mathrm{T}}^2 + \texttt{hdamp}^2} \tag{3}$$

to the singular part of the real radiation [30], where p_{T} is the transverse momentum of the $t\bar{t}$ system. The `hdamp` parameter is parametrised as `hdamp` $= h \cdot m_t$, and the factor h is tuned to the $t\bar{t}$ data. Previous studies showed that values of h between one and two lead to a good description of QCD radiation in $t\bar{t}$ events [31, 32]. The starting scale of the parton shower is set to the p_{T} of the $t\bar{t}$ system. In the MadGraph5_aMC@NLO generator, it is possible to change the upper scale for the MC subtraction term, which corresponds to the starting scale of the parton shower [22]. The upper scale for the MC subtraction term is set as a fraction of a reference scale, which corresponds to the invariant mass of the $t\bar{t}$ system. The parameters `frac_upp` and `frac_low`, determine the minimum and maximum fractions, respectively, of the reference scale, which are used as an upper limit for the MC subtraction term. The parameters `frac_upp` and `frac_low` are set to `frac_upp` $=$ `frac_low` $= f$, the sensitivity of the $t\bar{t}$ measurements to the f parameter is studied, and the optimal value is extracted from the data. Unlike the parton shower parameters $\alpha_s^{\mathrm{ISR}}(m_Z)$, $\alpha_s^{\mathrm{FSR}}(m_Z)$, and $p_{\mathrm{T,min}}^{\mathrm{FSR}}$, the parameters `hdamp`, `frac_upp` and `frac_low` are expected to be process dependent, and the results obtained are specific to $t\bar{t}$ production. In the tuning of the `hdamp` parameter in Powheg, and of the `frac_upp` and `frac_low` parameters in MadGraph5_aMC@NLO, the Pythia8 parton shower parameters are fixed to the values obtained by tuning Pythia8 to the $t\bar{t}$ measurements. This is based on the assumption that the effective values of $\alpha_s^{\mathrm{ISR}}(m_Z)$ and $\alpha_s^{\mathrm{FSR}}(m_Z)$ are not significantly affected by the inclusion of the NLO corrections to the calculations of the matrix elements of the $pp \to t\bar{t}$ process. Tables 1 and 2 show the parameters, the corresponding MC settings, and the ranges considered in the tuning for Pythia8 and for the NLO+PS generators, respectively.

The tuning is performed using Professor v1.4 [33] for the fit to the data, and Rivet v2.2.0 [34] for the implementation of the measurements. The method implemented in Professor permits the simultaneous tuning of several parameters by using an analytic approximation for the dependence of the physical observables on the model parameters, an idea first introduced in Ref. [13]. Polynomials of third-order are used to parametrise the response of the observables to the generator parameters, the coefficients in the polynomials are obtained by fitting MC predictions generated at a set of randomly selected parameter points, called anchor points. The number of anchor points used is 50 for one-parameter tuning, 100 for two-parameters tuning, and 400 for four-parameters tuning, with $2 \cdot 10^6$ dilepton $t\bar{t}$ events and 10^7 semileptonic $t\bar{t}$ events generated at each point. The optimal values of the model parameters are obtained with a standard χ^2 minimisation of the analytic approximation to the corresponding data using MINUIT [35].

Table 2: Parameters ranges used for the tuning of POWHEG+PYTHIA8 and MadGraph5_aMC@NLO+PYTHIA8, and the corresponding default values.

	POWHEG setting	Variation range	default
Real radiation damping	`hdamp` $= h \cdot m_t$	$0.5 \cdot m_t - 4.0 \cdot m_t$	∞
	MadGraph5_aMC@NLO setting		
Upper limit of the MC subtraction term	`frac_low` = `frac_upp` $= f$	0.2 – 1.0	`frac_low` = 0.1 `frac_upp` = 1.0

The MC statistical uncertainties are treated as uncorrelated and included in the definition of the χ^2 function. For the first time in the context of parton shower tuning in MC simulations, the correlation of the experimental uncertainties is included in the χ^2 minimisation. In presence of correlations, the χ^2 function is defined as:

$$\chi^2 = (\vec{x} - \vec{\mu})^T C^{-1} (\vec{x} - \vec{\mu}) \tag{4}$$

where $\vec{x}$ is the vector of data, $\vec{\mu}$ the interpolated MC prediction and C the covariance matrix of the data. Each source of systematic uncertainty is treated as fully correlated across the bins of each observable, and across the various observables of each of the three $t\bar{t}$ measurements. The measurement of the gap fraction has also a significant bin-to-bin statistical correlation, which is considered in the definition of the covariance matrix C. The MC statistical uncertainty of the $t\bar{t}$ +jets measurement is considered uncorrelated across bins.

3 Sensitivity study

As a first step in the process of tuning the MC to the $t\bar{t}$ measurements, a study of the sensitivity of the various observables to the parameters is performed. The results of the sensitivity study can guide the selection of the observables to use for tuning the ISR and FSR parameters, respectively, and the parameters of the NLO+PS generators.

The sensitivity of each observable bin to a set of parameters p_i, is estimated from the interpolated response of the observables to the parameters, with the following formula:

$$S_i = \frac{\partial MC(\vec{p})}{|MC(p_0)| + \epsilon w_{MC}} \frac{|p_{0,i}| + \epsilon w_{p_i}}{\partial p_i} \tag{5}$$

where p_0 is the centre of the parameters range, $MC(p_0)$ is the interpolated MC prediction at p_0 and the ϵ terms, set to 1% of the parameter range are introduced to avoid the ill defined case $MC(p_0) = 0, \partial p_i = 0$. w_{p_i} corresponds to 80% of the original sampling range and is used to construct w_{MC}.

Figure 1 shows the sensitivity of the differential $t\bar{t}$ cross sections as functions of jet multiplicity and jet transverse momentum, and of the gap fraction as a function of Q_0, to the PYTHIA8 parton shower parameters. Both measurements are mostly sensitive to the ISR parameters $\alpha_s^{\mathrm{ISR}}(m_Z)$ and $p_{\mathrm{T,damp}}^{\mathrm{ISR}}$, and

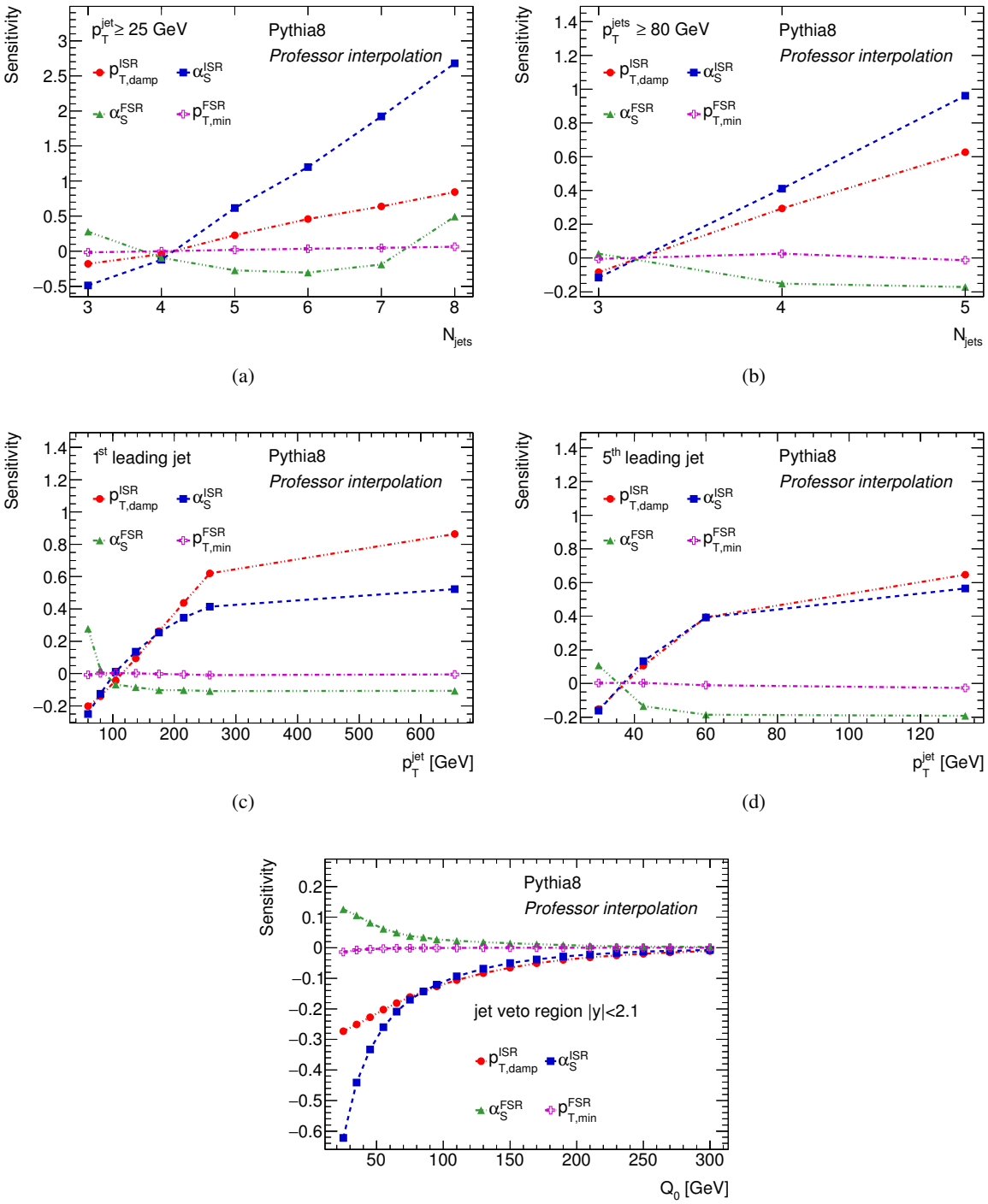

Figure 1: Sensitivity of the differential $t\bar{t}$ cross sections and $t\bar{t}$ gap fraction to the Pythia8 parton shower parameters $p_{T,damp}^{ISR}$ (red circles), $\alpha_s^{ISR}(m_Z)$ (blue squares), $\alpha_s^{FSR}(m_Z)$ (green triangles), and $p_{T,min}^{FSR}$ (magenta crosses). The sensitivities are shown as functions of (a) jet multiplicity for jets with $p_T^{jet} \geqslant 25$ GeV, (b) jet multiplicity for jets with $p_T^{jet} \geqslant 80$ GeV, (c) leading-jet transverse momentum, (d) 5th-leading jet transverse momentum, and (e) gap fraction as a function of Q_0.

Table 3: Tuning results of the $\alpha_s^{\mathrm{ISR}}(m_Z)$ and $p_{\mathrm{T,damp}}^{\mathrm{ISR}}$ Pythia8 parameters to the differential $t\bar{t}$ cross sections as functions of jet multiplicity and jet transverse momentum ($t\bar{t}$+jets), and to the gap fraction as a function of Q_0 ($t\bar{t}$ gap fraction), using the 4C tune as baseline. The '-' symbol is used in case the setting is not applicable.

Parameter	$t\bar{t}$+jets	$t\bar{t}$ gap fraction	$t\bar{t}$+jets and $t\bar{t}$ gap fraction	4C	AZ
$\alpha_s^{\mathrm{ISR}}(m_Z)$	0.130 ± 0.005	$0.129^{+0.012}_{-0.010}$	0.130 ± 0.005	0.137	$0.1237^{+0.0018}_{-0.0002}$
$p_{\mathrm{T,damp}}^{\mathrm{ISR}}$	$1.33^{+0.11}_{-0.10}$	$1.31^{+0.21}_{-0.18}$	$1.32^{+0.10}_{-0.09}$	-	-
χ^2_{min}/dof	30/19	10/16	40/37		

to less extent to the FSR parameter $\alpha_s^{\mathrm{FSR}}(m_Z)$. Figure 2 shows the sensitivity of the light-jet shapes to the Pythia8 parton shower parameters. The light-jet shapes are mostly sensitive to the FSR parameter $\alpha_s^{\mathrm{FSR}}(m_Z)$, some sensitivity is observed also to the FSR parameter $p_{\mathrm{T,min}}^{\mathrm{FSR}}$ and to the ISR parameter $\alpha_s^{\mathrm{ISR}}(m_Z)$. Similar sensitivities are observed for the b-jet shapes.

Based on the results of the sensitivity study, the differential $t\bar{t}$ cross sections as functions of jet multiplicity and jet transverse momentum, and the gap fraction as a function of Q_0 are used to study the consistency of the ISR parameters with previous tunes to the Z boson transverse momentum, whereas the jet-shapes are used to study the consistency of the FSR parameters with previous tunes to the LEP measurements. However, the sensitivity study also shows that the ISR and FSR parameters are not completely decoupled: the observables sensitive to the ISR parameters have some sensitivity to $\alpha_s^{\mathrm{FSR}}(m_Z)$, and the observables used to tune the FSR parameters have some sensitivity to $\alpha_s^{\mathrm{ISR}}(m_Z)$. To account for such an interplay between ISR and FSR parameters, a simultaneous tune of ISR and FSR parameters is performed using all the measurements.

Figure 3 shows the sensitivity of the differential $t\bar{t}$ cross sections as functions of jet multiplicity and jet transverse momentum, and of the gap fraction as a function of Q_0, to the h and f parameters of Powheg and MadGraph5_aMC@NLO. The light- and b-jet shapes have negligible sensitivity to the h and f parameters, hence only the $t\bar{t}$ + jets differential cross sections and the $t\bar{t}$ gap fraction measurement are used in the tuning of these parameters.

4 Initial-state radiation

As shown in the previous section, the differential $t\bar{t}$ cross sections as functions of jet multiplicity and jet transverse momentum, and the gap fraction as a function of Q_0, are sensitive to the ISR parameters $\alpha_s^{\mathrm{ISR}}(m_Z)$ and $p_{\mathrm{T,damp}}^{\mathrm{ISR}}$. While the fudge factor for the damping of ISR, $p_{\mathrm{T,damp}}^{\mathrm{ISR}}$, is introduced in the specific case of the $t\bar{t}$ production to compensate for missing matrix-element corrections in the Pythia8 MC [23], the $\alpha_s^{\mathrm{ISR}}(m_Z)$ parameter is expected to be universal across different processes. In particular, by comparing the value constrained in $t\bar{t}$ production, to the value preferred by the transverse momentum spectrum of Z bosons produced in pp collisions [10], the validity of the ISR parton shower model can be tested in processes dominated by different initial states: gluon-gluon for $t\bar{t}$ production and quark-antiquark for Z production. Table 3 shows the results of the tuning of the ISR parameters to the $t\bar{t}$ measurements using the 4C tune as baseline. The results are compared to the AZ tune to the Z boson transverse momentum spectrum [10], which was performed using the same 4C tune as baseline, and the same CTEQ6L1 PDF set. Independent tuning to the differential $t\bar{t}$ cross sections as functions of jet

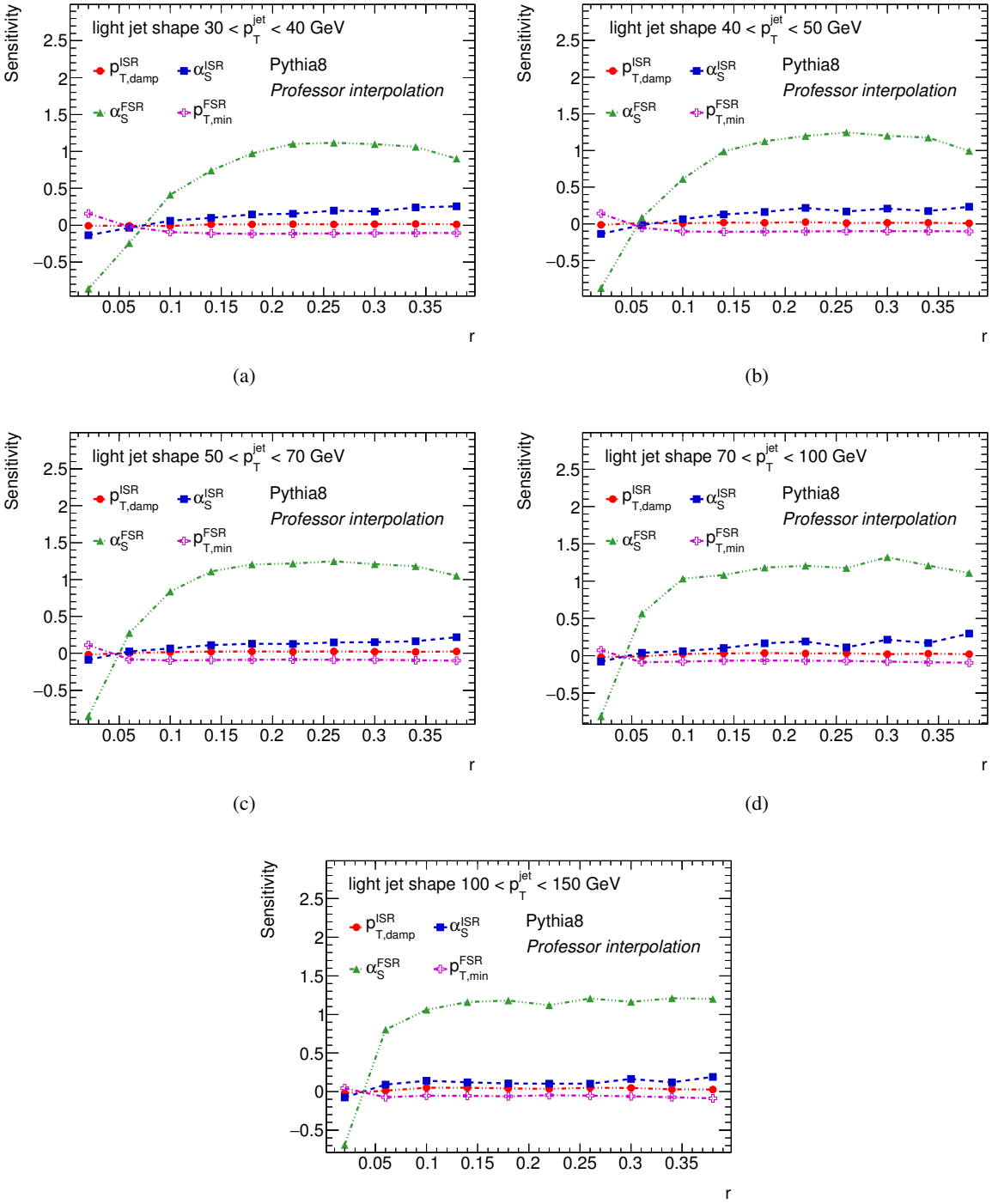

Figure 2: Sensitivity of the light-jet shapes to the PYTHIA8 parton shower parameters $p_{\mathrm{T,damp}}^{\mathrm{ISR}}$ (red circles), $\alpha_s^{\mathrm{ISR}}(m_Z)$ (blue squares), $\alpha_s^{\mathrm{FSR}}(m_Z)$ (green triangles), and $p_{\mathrm{T,min}}^{\mathrm{FSR}}$ (magenta crosses). The sensitivities are shown as functions of the light-jet radius r for jets with (a) $30 < p_{\mathrm{T}}^{\mathrm{jet}} < 40$ GeV, (b) $40 < p_{\mathrm{T}}^{\mathrm{jet}} < 50$ GeV, (c) $50 < p_{\mathrm{T}}^{\mathrm{jet}} < 70$ GeV, (d) $70 < p_{\mathrm{T}}^{\mathrm{jet}} < 100$ GeV, and (e) $100 < p_{\mathrm{T}}^{\mathrm{jet}} < 150$ GeV.

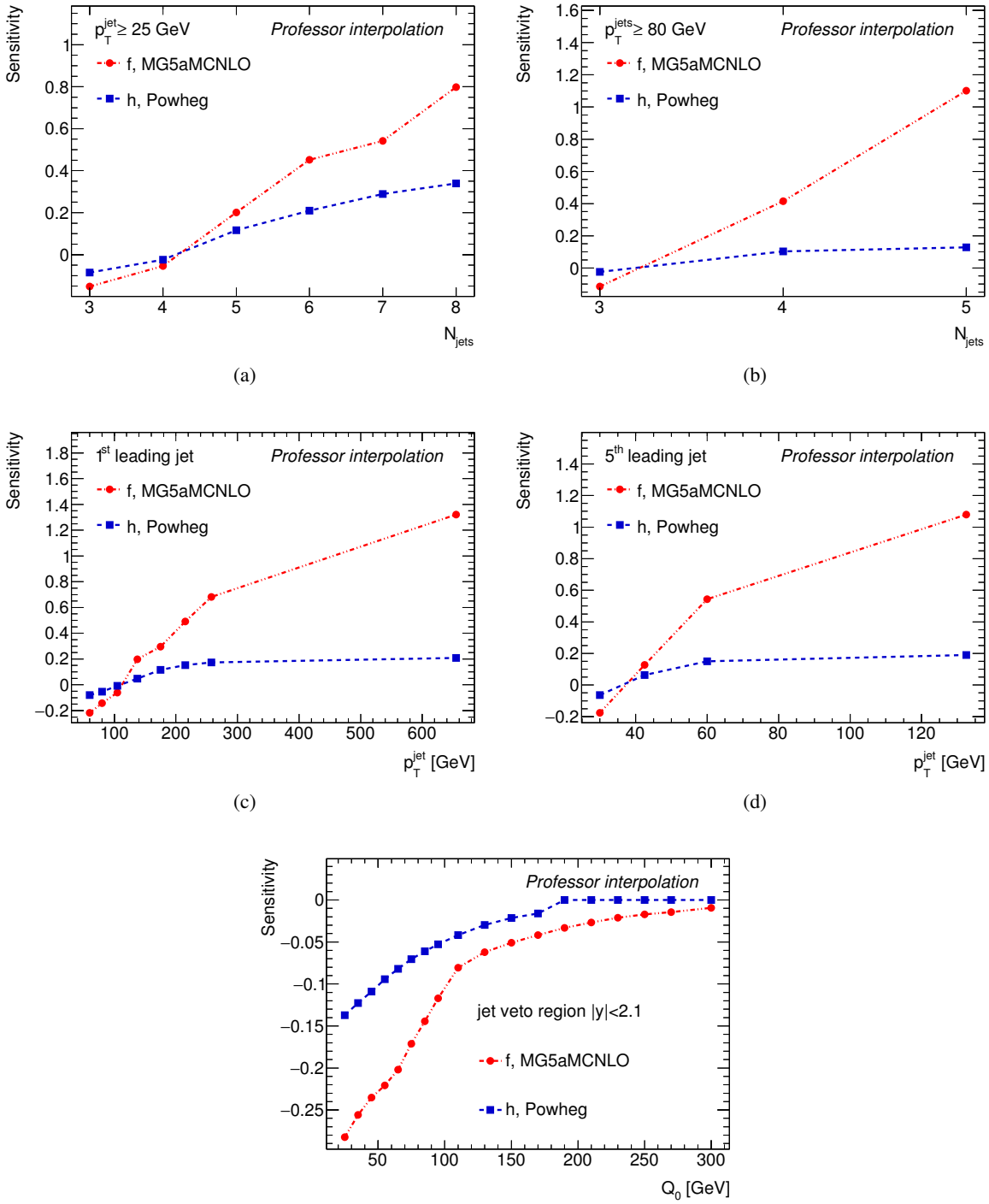

Figure 3: Sensitivity of the $t\bar{t}$ measurements to the h (red circles) and f (blue squares) parameters of POWHEG and MadGraph5_aMC@NLO, respectively. The sensitivities are shown as functions of the differential $t\bar{t}$ cross sections as functions of (a) jet multiplicity for jets with $p_T^{jet} \geqslant 25$ GeV, (b) jet multiplicity for jets with $p_T^{jet} \geqslant 80$ GeV, (c) leading-jet transverse momentum, (d) 5th-leading jet transverse momentum, and (e) gap fraction as a function of Q_0.

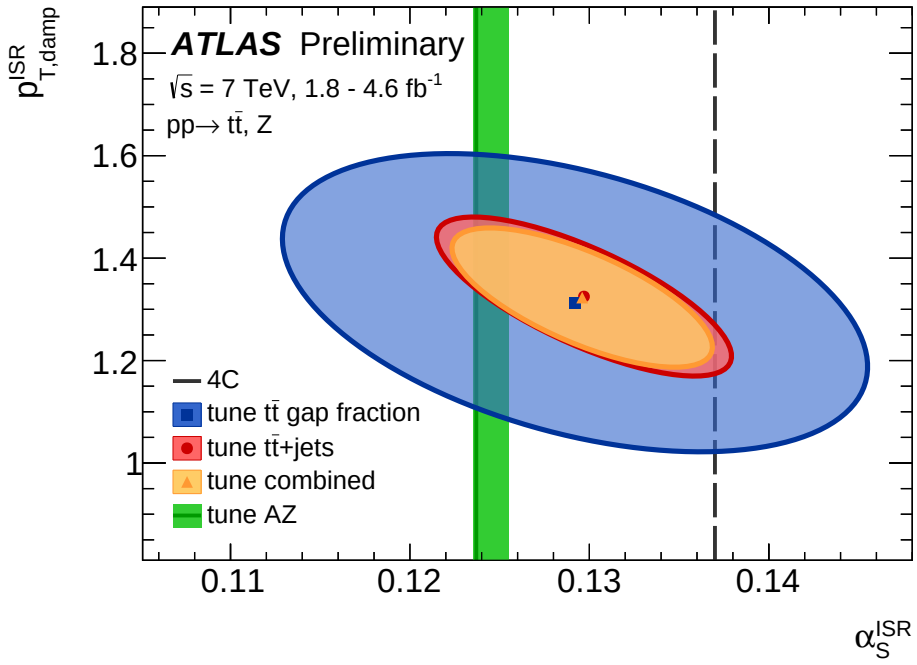

Figure 4: Optimal values of the Pythia8 ISR parameters $\alpha_s^{\mathrm{ISR}}(m_Z)$ and $p_{\mathrm{T,damp}}^{\mathrm{ISR}}$ obtained from tunes to the $t\bar{t}$ gap fraction (blue square), $t\bar{t}$ +jets (red circle) and their combination (yellow triangle) compared to the value of $\alpha_s^{\mathrm{ISR}}(m_Z)$ of the AZ (green line) and 4C (black dashed line) tunes. The ellipses correspond to the 68% confidence interval, and the green band shows the uncertainty on the value of $\alpha_s^{\mathrm{ISR}}(m_Z)$ in the AZ tune.

Table 4: Tuning results of $\alpha_s^{\mathrm{ISR}}(m_Z)$ and $p_{\mathrm{T,damp}}^{\mathrm{ISR}}$ Pythia8 parameters to the differential $t\bar{t}$ cross sections as functions of jet multiplicity and jet transverse momentum ($t\bar{t}$+jets), and to the gap fraction as a function of Q_0 ($t\bar{t}$ gap fraction), using the Monash tune as baseline. The '-' symbol is used in case the setting is not applicable.

Parameter	$t\bar{t}$+jets	$t\bar{t}$ gap fraction	$t\bar{t}$+jets and $t\bar{t}$ gap fraction (ATTBAR-ISR)	Monash
$\alpha_s^{\mathrm{ISR}}(m_Z)$	0.124 ± 0.006	0.124 ± 0.010	$0.124^{+0.005}_{-0.006}$	0.137
$p_{\mathrm{T,damp}}^{\mathrm{ISR}}$	1.13 ± 0.09	$1.19^{+0.17}_{-0.15}$	1.14 ± 0.08	-
χ^2_{min}/dof	24/19	10/16	34/37	

multiplicity and jet transverse momentum, and to the gap fraction as a function of Q_0, show very similar results for the optimised parameters. The value of $\alpha_s^{\mathrm{ISR}}(m_Z)$ obtained from the tune to both measurements is in rather good agreement with the value of the AZ tune. Figure 4 shows the comparison between the optimal values of the ISR tunes to the $t\bar{t}$ data and the AZ tune, which is constrained to the ATLAS measurement of the Z boson transverse momentum at $\sqrt{s} = 7$ TeV. The 68% confidence interval in the $\alpha_s^{\mathrm{ISR}}(m_Z)$ and $p_{\mathrm{T,damp}}^{\mathrm{ISR}}$ space is obtained from the Hessian matrix of the χ^2 at the minimum.

Table 4 shows the results of the tuning of the ISR parameters to the $t\bar{t}$ measurements using the Monash tune as baseline and the NNPDF2.3 LO PDF set. The optimal values of the ISR parameters obtained using Monash as the baseline tune are slightly different to those obtained with 4C, and the value of the χ^2 is up to six points better in the case of Monash. The most relevant difference between the 4C and Monash tunes, which affects the results of the tuning of ISR, is the different PDF set, CTEQ6L1 in 4C

Table 5: Tuning results of the $\alpha_s^{\mathrm{FSR}}(m_Z)$ Pythia8 parameter to the differential light- and b-jet shapes in $t\bar{t}$ events, using the 4C tune as baseline.

Parameter	light-jet shapes	b-jet shapes	4C
$\alpha_s^{\mathrm{FSR}}(m_Z)$	0.131 ± 0.001	0.126 ± 0.001	0.1383
χ^2_{min}/dof	64/49	284/49	

Table 6: Tuning results of the $\alpha_s^{\mathrm{FSR}}(m_Z)$ Pythia8 parameter to the differential light- and b-jet shapes in $t\bar{t}$ events, using the Monash tune as baseline.

Parameter	light-jet shapes	b-jet shapes	Monash
$\alpha_s^{\mathrm{FSR}}(m_Z)$	0.125 ± 0.001	0.121 ± 0.001	0.1365
χ^2_{min}/dof	71/49	219/49	

and NNPDF2.3 LO in Monash. The tune of the ISR parameters to both the $t\bar{t}$ + jets and $t\bar{t}$ gap fraction measurements, with the Monash tune as baseline, is referred to as ATTBAR-ISR. Figure 5 shows the $t\bar{t}$ measurements compared to the Pythia8 predictions with the Monash and ATTBAR-ISR tunes. A very good agreement between the data and the ATTBAR-ISR tune is observed in all the distributions.

5 Final-state radiation

The light- and b-jet shapes measured in $t\bar{t}$ events are sensitive to the value of $\alpha_s^{\mathrm{FSR}}(m_Z)$, and, to less extent, to the value of $p_{\mathrm{T,min}}^{\mathrm{FSR}}$. The measurements can be used to tune such FSR parameters, and the optimal values can be compared to the corresponding values tuned to the event shapes in Z boson hadronic decay as measured at LEP. In Ref. [2], values of $\alpha_s^{\mathrm{FSR}}(m_Z)$ in the range $0.135 - 0.140$ are suggested by comparing Pythia8 predictions and the LEP data [11], and a Professor tune of Pythia8 hadronisation and FSR parameters to LEP measurements [12–14] returns 0.139 as optimal value of $\alpha_s^{\mathrm{FSR}}(m_Z)$ [36]. Tables 5 and 6 show the results of the tuning of the FSR parameter $\alpha_s^{\mathrm{FSR}}(m_Z)$ to the light- and b-jet shapes in $t\bar{t}$ events, using the 4C and Monash tune as baselines, respectively. The results show tension in the value of $\alpha_s^{\mathrm{FSR}}(m_Z)$ between light- and b-jet shapes. The χ^2_{min}/dof is close to unity in the case of the light-jet shapes, whereas it is larger than 4 for the b-jet shapes, pointing to a mismodelling of the latter. Despite the better χ^2_{min}/dof of the tune of $\alpha_s^{\mathrm{FSR}}(m_Z)$ to the light-jet shapes in $t\bar{t}$ events, the optimal values of $\alpha_s^{\mathrm{FSR}}(m_Z) = 0.131 \pm 0.001$ and $\alpha_s^{\mathrm{FSR}}(m_Z) = 0.125 \pm 0.001$ show some difference with respect to the values preferred by the LEP measurements of event shapes in Z boson hadronic decay.

Tables 7 and 8 show the results of the tuning of the FSR parameters $\alpha_s^{\mathrm{FSR}}(m_Z)$ and $p_{\mathrm{T,min}}^{\mathrm{FSR}}$ to the light-jet shapes in $t\bar{t}$ events, using the 4C and Monash tune as baselines, respectively. The inclusion of $p_{\mathrm{T,min}}^{\mathrm{FSR}}$ as a free parameter in the fit does not improve the mismodelling of the b-jet shapes, and the corresponding tunes to the b-jet shapes do not converge within the sampled range of parameters.

With the addition of $p_{\mathrm{T,min}}^{\mathrm{FSR}}$ as a free parameter in the fit, the χ^2 of the two FSR tunes to the light-jet shapes are about ten points lower, and the resulting values of $\alpha_s^{\mathrm{FSR}}(m_Z)$ are compatible with the values preferred by the LEP event shapes. However, the optimal value of $p_{\mathrm{T,min}}^{\mathrm{FSR}}$ is rather high with respect to the values used in the baseline tunes, 0.88 GeV and 1.31 GeV compared to 0.4 GeV and 0.5 GeV for the 4C and

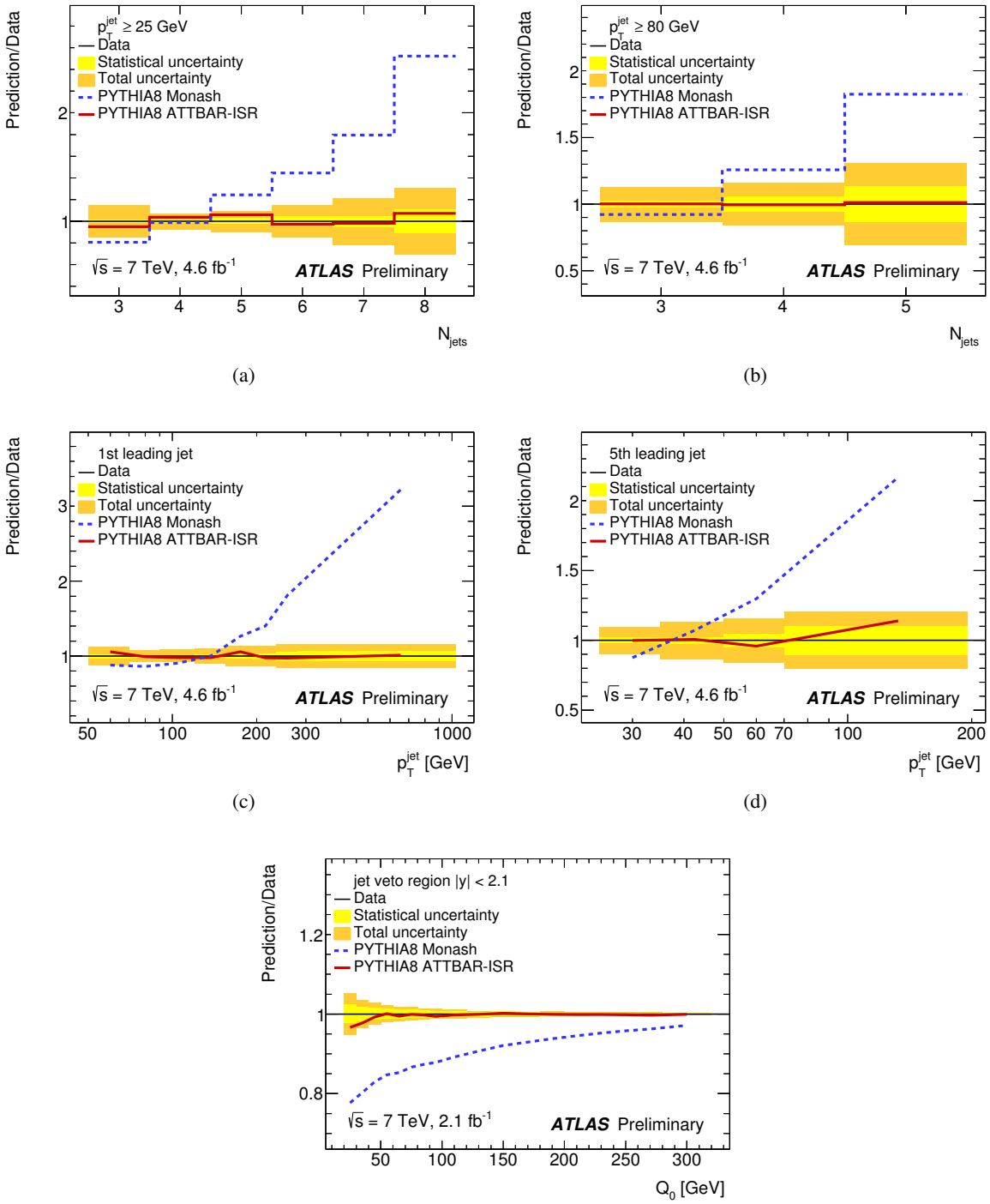

Figure 5: Predictions of PYTHIA8 with the ATTBAR-ISR (red continuous line) and Monash (blue dashed line) tunes, compared to the measured differential $t\bar{t}$ cross sections as functions of (a) jet multiplicity for jets with $p_T^{jet} \geqslant 25$ GeV, (b) jet multiplicity for jets with $p_T^{jet} \geqslant 80$ GeV, (c) leading-jet transverse momentum, (d) 5th-leading jet transverse momentum, and (e) gap fraction as a function of Q_0. The relative statistical (yellow band) and total (orange band) experimental uncertainties are shown.

Table 7: Tuning results of the $\alpha_s^{\mathrm{FSR}}(m_Z)$ and $p_{\mathrm{T,min}}^{\mathrm{FSR}}$ Pythia8 parameters to the differential light-jet shapes in $t\bar{t}$ events, using the 4C tune as baseline.

Parameter	light-jet shapes	4C
$\alpha_s^{\mathrm{FSR}}(m_Z)$	$0.137^{+0.003}_{-0.002}$	0.1383
$p_{\mathrm{T,min}}^{\mathrm{FSR}}$ [GeV]	0.88 ± 0.16	0.4
χ^2_{min}/dof	55/49	

Table 8: Tuning results of the $\alpha_s^{\mathrm{FSR}}(m_Z)$ and $p_{\mathrm{T,min}}^{\mathrm{FSR}}$ Pythia8 parameters to the differential light-jet shapes in $t\bar{t}$ events, using the Monash tune as baseline.

Parameter	light-jet shapes (ATTBAR-FSR)	Monash
$\alpha_s^{\mathrm{FSR}}(m_Z)$	0.135 ± 0.003	0.1365
$p_{\mathrm{T,min}}^{\mathrm{FSR}}$ [GeV]	$1.31^{+0.18}_{-0.20}$	0.5
χ^2_{min}/dof	57/49	

Monash tunes, respectively. Although the addition of $p_{\mathrm{T,min}}^{\mathrm{FSR}}$ as a free parameter restored compatibility in the value of $\alpha_s^{\mathrm{FSR}}(m_Z)$ between the tunes to the light-jet shapes in $t\bar{t}$ events, and the tunes based on LEP event shapes, the resulting higher values of $p_{\mathrm{T,min}}^{\mathrm{FSR}}$ leave an undesirable gap between the FSR cut-off and the scale of hadronisation [2]. Indeed, the scale of the p_{T} kicks involved in string breaking of the Pythia8 hadronisation model (corresponding to the `StringPT:sigma` parameter) is set to $\sigma_\perp = 0.304$ GeV in the 4C tune, and $\sigma_\perp = 0.335$ GeV in the Monash tune. The result of $p_{\mathrm{T,min}}^{\mathrm{FSR}}$ is also incompatible with the determination of this parameter from LEP data of Ref. [36], which is 0.41 GeV. The difference in the preferred values of $p_{\mathrm{T,min}}^{\mathrm{FSR}}$ suggests that there is a residual tension between the light-jet shapes in $t\bar{t}$ events and the LEP event shapes. Further studies on the impact of changing parameters of the fragmentation function, of different colour reconnection models [37], and of NLO corrections in W boson hadronic decays [38], could cast light on the nature of such a tension.

The tune of the FSR parameters to the light-jet shapes in $t\bar{t}$ events, with the Monash tune as baseline, shown in Table 8, is referred to as ATTBAR-FSR. Figure 6 shows the measurements of light-jet shapes in $t\bar{t}$ events, compared to the Pythia8 predictions with the Monash and ATTBAR-FSR tunes. The b-jet shapes differential distributions are compared in Fig. 7 to the Pythia8 predictions of the same Monash and ATTBAR-FSR tunes. The comparison shows a mismodelling of the b-jets shapes, which are predicted to be wider than observed in the data. The mismodelling is more pronounced at high jet p_{T} above 70 GeV and at large angle r above 0.1. The NLO corrections in top quark decays, which has been included in Powheg [38], have an impact on the b-quark fragmentation function, and could improve the agreement between the measurements and the predictions.

6 Simultaneous tune of ISR and FSR

As observed in Section 3, the observables used for tuning the ISR parameters have some sensitivity to $\alpha_s^{\mathrm{FSR}}(m_Z)$, and the observables used to tune the FSR parameters have some sensitivity to $\alpha_s^{\mathrm{ISR}}(m_Z)$. To account for the interplay between ISR and FSR parameters, a simultaneous tune of ISR and FSR

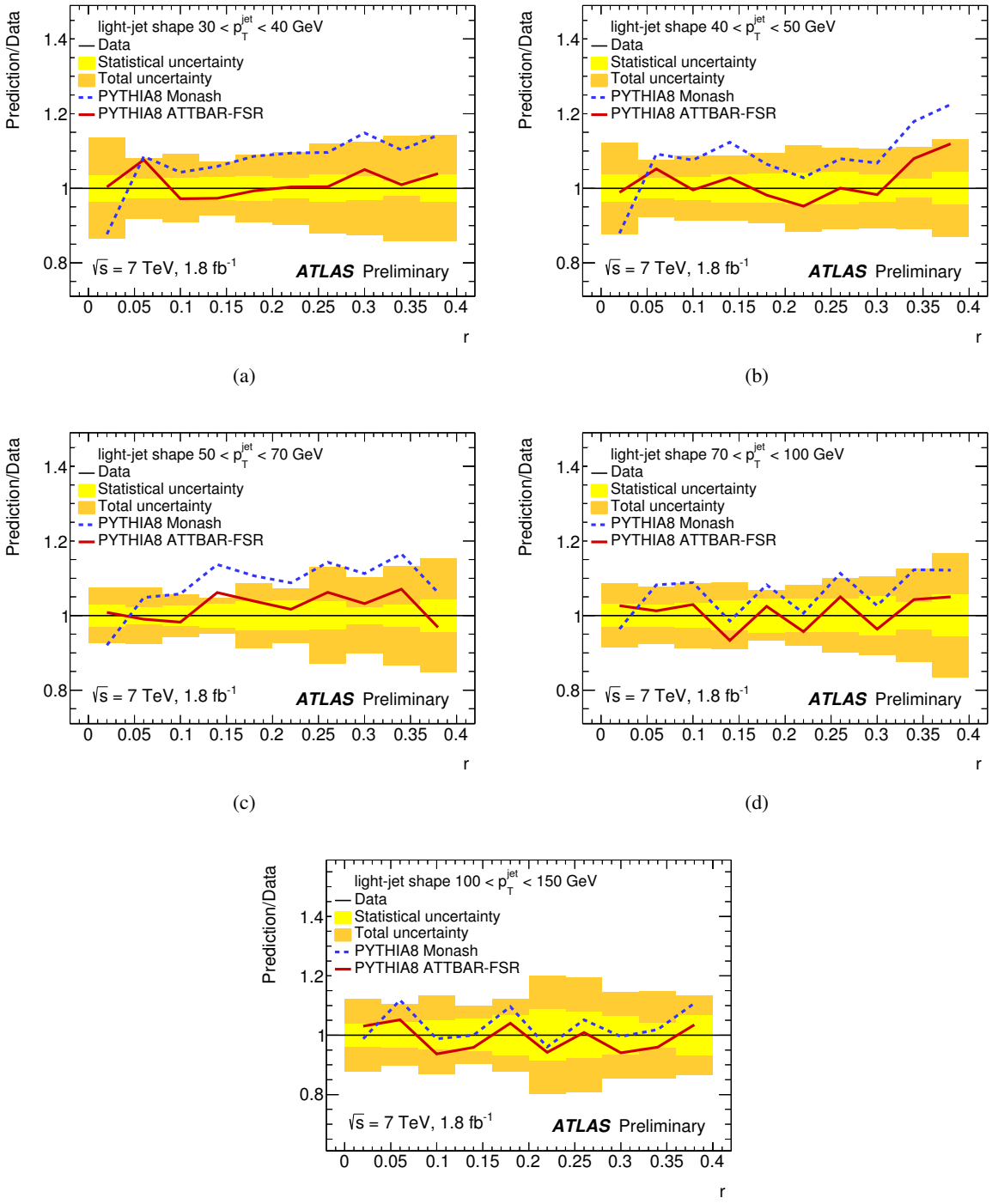

Figure 6: Predictions of PYTHIA8 with the ATTBAR-FSR (red continuous line) and Monash (blue dashed line) tunes, compared to the light-jet shapes as functions of the jet radius r for jets with (a) $30 < p_{\mathrm{T}}^{\mathrm{jet}} < 40$ GeV, (b) $40 < p_{\mathrm{T}}^{\mathrm{jet}} < 50$ GeV, (c) $50 < p_{\mathrm{T}}^{\mathrm{jet}} < 70$ GeV, (d) $70 < p_{\mathrm{T}}^{\mathrm{jet}} < 100$ GeV, and (e) $100 < p_{\mathrm{T}}^{\mathrm{jet}} < 150$ GeV. The relative statistical (yellow band) and total (orange band) experimental uncertainties are shown.

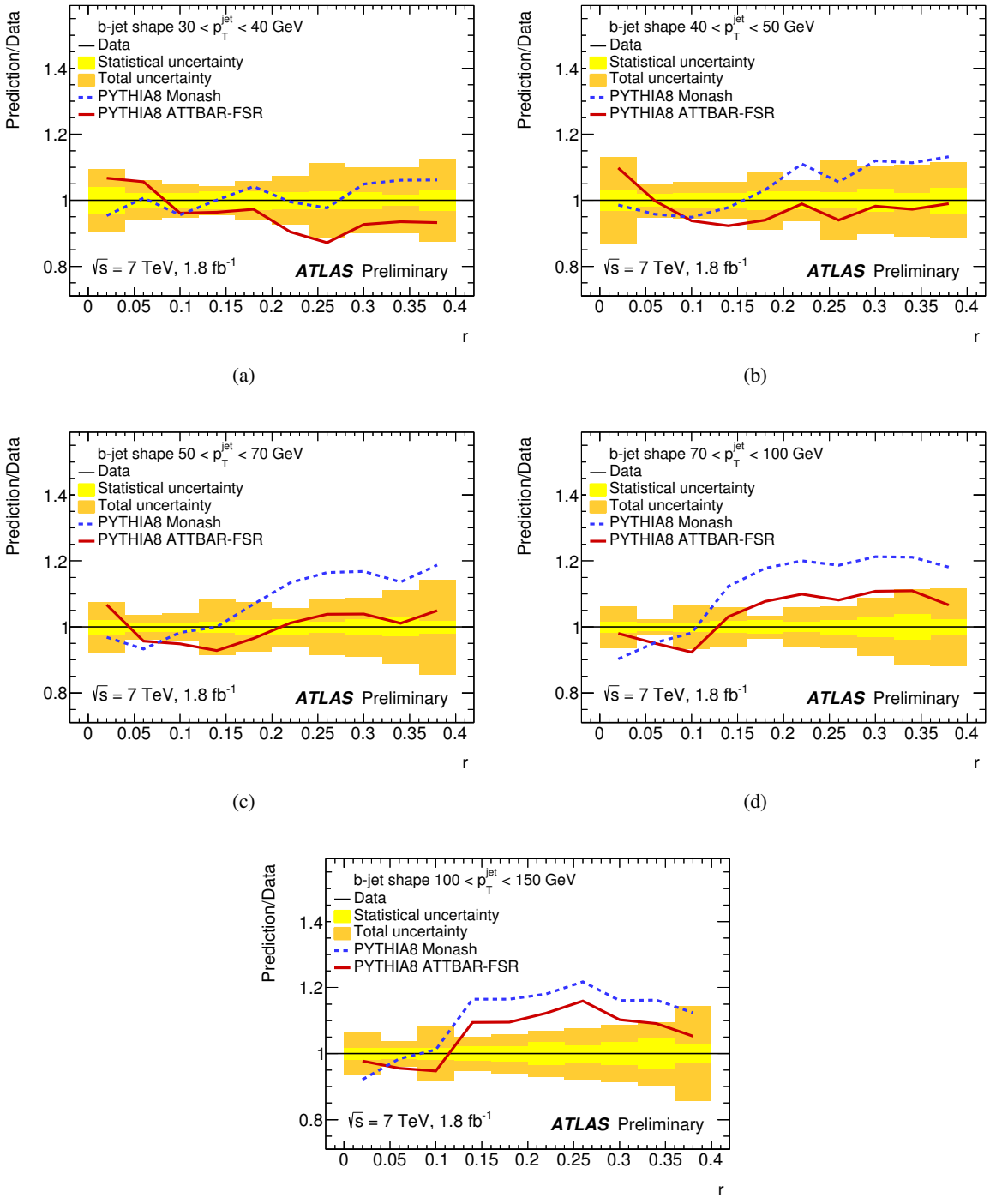

Figure 7: Predictions of Pythia8 with the ATTBAR-FSR (red continuous line) and Monash (blue dashed line) tunes, compared to the b-jet shapes as functions of the jet radius r for jets with (a) $30 < p_{\mathrm{T}}^{\mathrm{jet}} < 40$ GeV, (b) $40 < p_{\mathrm{T}}^{\mathrm{jet}} < 50$ GeV, (c) $50 < p_{\mathrm{T}}^{\mathrm{jet}} < 70$ GeV, (d) $70 < p_{\mathrm{T}}^{\mathrm{jet}} < 100$ GeV, and (e) $100 < p_{\mathrm{T}}^{\mathrm{jet}} < 150$ GeV. The relative statistical (yellow band) and total (orange band) experimental uncertainties are shown.

Table 9: Tuning results of the Pythia8 ISR and FSR parameters to the differential $t\bar{t}$ cross sections as functions of jet multiplicity and jet transverse momentum, the gap fraction as a function of Q_0, and the differential light-jet shapes in $t\bar{t}$ events, using the 4C tune as baseline. The '-' symbol is used in case the setting is not applicable.

Parameter	ATLAS $t\bar{t}$ measurements	4C
$\alpha_s^{\mathrm{ISR}}(m_Z)$	0.127 ± 0.004	0.137
$p_{\mathrm{T,damp}}^{\mathrm{ISR}}$	$1.36^{+0.09}_{-0.08}$	-
$\alpha_s^{\mathrm{FSR}}(m_Z)$	0.139 ± 0.002	0.1383
$p_{\mathrm{T,min}}^{\mathrm{FSR}}$ [GeV]	$0.85^{+0.16}_{-0.17}$	0.4
χ^2_{min}/dof	97/85	

Table 10: Tuning results of the Pythia8 ISR and FSR parameters to the differential $t\bar{t}$ cross sections as functions of jet multiplicity and jet transverse momentum, the gap fraction as a function of Q_0, and the differential light-jet shapes in $t\bar{t}$ events, using the Monash tune as baseline. The '-' symbol is used in case the setting is not applicable.

Parameter	ATLAS $t\bar{t}$ measurements (ATTBAR)	Monash
$\alpha_s^{\mathrm{ISR}}(m_Z)$	0.121 ± 0.004	0.1365
$p_{\mathrm{T,damp}}^{\mathrm{ISR}}$	$1.18^{+0.08}_{-0.07}$	-
$\alpha_s^{\mathrm{FSR}}(m_Z)$	0.137 ± 0.003	0.1365
$p_{\mathrm{T,min}}^{\mathrm{FSR}}$ [GeV]	1.26 ± 0.17	0.5
χ^2_{min}/dof	92/85	

parameters is performed using the differential $t\bar{t}$ cross sections as functions of jet multiplicity and jet transverse momentum, the gap fraction as a function of Q_0, and the differential light-jet shapes in $t\bar{t}$ events. The differential b-jet shapes in $t\bar{t}$ events are not used, since they are not well modelled by the Pythia8 MC, as shown in the previous Section.

Tables 9 and 10 show the results of the tuning of the ISR and FSR parameters to the $t\bar{t}$ measurements using the 4C and Monash tunes as baselines, respectively. The results of the simultaneous tunes of ISR and FSR are in rather good agreement with the results of the independent tunes. The overall χ^2_{min}/dof is 97/85 when using the 4C tune as baseline, and 92/85 with the Monash tune as baseline. The tune of the ISR and FSR parameters to the $t\bar{t}$ data events, with the Monash tune as baseline, shown in Table 10, is referred to as ATTBAR. The Pythia8 predictions with the ATTBAR tune are very similar to those of the ATTBAR-ISR and ATTBAR-FSR tunes, they are shown in Figs. 11, 13, and 14.

In order to check the impact of accounting for uncertainties correlation in the χ^2 definition, a tune is performed with the same conditions of the ATTBAR tune, but considering the total experimental uncertainties as fully uncorrelated. Table 11 shows the comparison between the ATTBAR tune, which is based on the uncertainties correlation model described in Section 2, and a corresponding tune without uncertainties correlations. The optimal parameters of the two tunes are in good agreement, but the uncertainties of the parameters are up to 50% lower in the ATTBAR tune. If correlations are not considered the tune yields a very small value of χ^2_{min}/dof, which is typically an indication of overestimated uncertainties. Only in ATTBAR the value of χ^2_{min}/dof is close to unity, a prerequisite to give a proper statistical meaning to the parameters values and their uncertainties. Figure 8 shows the correlations of the parton shower parameters of the ATTBAR tune, evaluated from the Hessian matrix at the minimum of the χ^2 function.

Table 11: The optimal parameters and their uncertainties as determined in the ATTBAR tune and in a tune performed without uncertainties correlations.

Parameter	ATTBAR	Tune without uncertainties correlations
$\alpha_s^{\mathrm{ISR}}(m_Z)$	0.121 ± 0.004	$0.118^{+0.007}_{-0.006}$
$p_{\mathrm{T,damp}}^{\mathrm{ISR}}$	$1.18^{+0.08}_{-0.07}$	$1.17^{+0.10}_{-0.09}$
$\alpha_s^{\mathrm{FSR}}(m_Z)$	0.137 ± 0.003	$0.138^{+0.006}_{-0.005}$
$p_{\mathrm{T,min}}^{\mathrm{FSR}}$ [GeV]	1.26 ± 0.17	1.35 ± 0.35
χ^2_{min}/dof	92/85	13/85

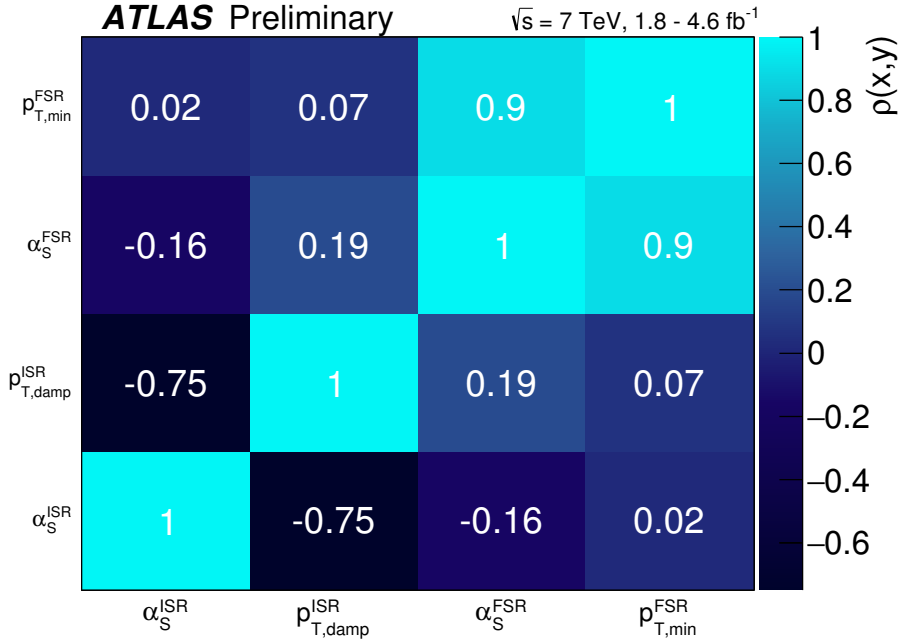

Figure 8: Parameters correlations $\rho(x, y)$ as evaluated from the Hessian matrix at χ^2_{min}, for the Pythia8 ATTBAR tune.

The variations of the ISR and FSR parameters induce a change in the overall energy and particle flow, which affects the underlying event activity. Measurements of the underlying event in the $t\bar{t}$ final state could be used to tune the multi-parton-interaction (MPI) parameters, but only a measurement from CMS was performed [39], which is a preliminary result. Assuming that the MPI model can describe simultaneously both $t\bar{t}$ and Z boson production, the change in the energy and particle flow is compensated by adjusting the MPI cut-off to match the inclusive charged particle production and energy flow in Z/γ^* underlying event data measured by ATLAS at $\sqrt{s} = 7$ TeV [40]. The MPI cut-off in ATTBAR is changed from 2.28 GeV, the value in the Monash tune, to 2.16 GeV. The same value of the MPI cut-off is used also for the NLO+PS predictions.

Table 12: Global-recoil and local-recoil settings of PYTHIA8 for the MadGraph5_aMC@NLO+PYTHIA8 generator. The '-' symbol is used in case the setting is not applicable.

PYTHIA8 setting	Global recoil	Local recoil
`SpaceShower:pTmaxMatch`	1	1
`SpaceShower:MEcorrections`	off	off
`TimeShower:MEcorrections`	off	off
`TimeShower:globalRecoil`	on	off
`TimeShower:globalRecoilMode`	2	-
`TimeShower:nMaxGlobalBranch`	1	-
`TimeShower:nPartonsInBorn`	2	-
`TimeShower:limitPTmaxGlobal`	on	-

7 Tune of the MadGraph5_aMC@NLO generator

The simultaneous ISR and FSR PYTHIA8 tune to the $t\bar{t}$ measurements, ATTBAR, is applied to the MadGraph5_aMC@NLO generator, with the exception of the $p_{\mathrm{T,damp}}^{\mathrm{ISR}}$ parameter. The parameters of MadGraph5_aMC@NLO which set the upper scale of the MC subtraction term, and the starting scale of the parton shower, are tuned to the $t\bar{t}$ data. The parameters `frac_upp` and `frac_low` of MadGraph5_aMC@NLO correspond, respectively, to the maximum and minimum fractions of a reference scale, for the upper scale of the MC subtraction term, where the reference scale is set to the invariant mass of the $t\bar{t}$ system. The best agreement with the data is found by fixing `frac_upp` and `frac_low` to the same common value f, and by tuning f to the differential $t\bar{t}$ cross sections as functions of jet multiplicity and jet transverse momentum, and to the gap fraction as a function of Q_0. When interfacing MadGraph5_aMC@NLO to PYTHIA8, the FSR algorithm should employ, at least for the first emission, a *global-recoil* strategy, in which the recoil of the FSR radiation is shared between all partons in the final state. The global-recoil strategy of FSR, which is opposite to the default dipole style local-recoil strategy, is needed to avoid double counting with the MC subtraction term of the MadGraph5_aMC@NLO generator. The matrix-element corrections to ISR and FSR are disabled in PYTHIA8, so as to obtain a process-independent emission rate which matches the MadGraph5_aMC@NLO subtraction term.

The tuning of the f parameter of MadGraph5_aMC@NLO is performed in two configurations: with the recommended settings for the global recoil, and with the global recoil option disabled (local recoil). The settings for the two configurations are listed in Table 12. Tables 13 and 14 show the results of tuning the parameter f to the differential $t\bar{t}$ cross sections as functions of jet multiplicity and jet transverse momentum, and to the gap fraction as a function of Q_0, using the ATTBAR tune, for the global- and local-recoil configurations, respectively. The values of f obtained by tuning to the $t\bar{t}$ + jets measurements are consistent with the values obtained by tuning to the $t\bar{t}$ gap fraction. The values of f obtained by tuning to both measurements, are $f = 0.58 \pm 0.03$ and $f = 0.54 \pm 0.03$ for the global- and local-recoil configurations, respectively. The tune of the f parameter to the $t\bar{t}$ data, with the ATTBAR tune and the local-recoil PYTHIA8 configuration, shown in Table 14, is referred to as ATTBAR-MG5aMCNLO.

Figure 9 shows the $t\bar{t}$ measurements compared to the MadGraph5_aMC@NLO+PYTHIA8 predictions with the Monash tune and the global-recoil configuration, f-tuned predictions with the ATTBAR tune and the

Table 13: Tuning results of the MadGraph5_aMC@NLO `frac_upp` = `frac_low` = f parameter to the differential $t\bar{t}$ cross sections as functions of jet multiplicity and jet transverse momentum ($t\bar{t}$+jets), and to the gap fraction as a function of Q_0 ($t\bar{t}$ gap fraction), using the ATTBAR tune, and the global-recoil configuration.

Parameter	$t\bar{t}$+jets	$t\bar{t}$ gap fraction	$t\bar{t}$+jets and $t\bar{t}$ gap fraction
f	0.58 ± 0.03	$0.53^{+0.09}_{-0.08}$	0.57 ± 0.03
χ^2_{min}/dof	43/20	14/17	57/38

Table 14: Tuning results of the MadGraph5_aMC@NLO `frac_upp` = `frac_low` = f parameter without using the global recoil settings to the differential $t\bar{t}$ cross sections as functions of jet multiplicity and jet transverse momentum ($t\bar{t}$+jets), and to the gap fraction as a function of Q_0 ($t\bar{t}$ gap fraction), using the ATTBAR tune, and the local-recoil configuration.

Parameter	$t\bar{t}$+jets	$t\bar{t}$ gap fraction	$t\bar{t}$+jets and $t\bar{t}$ gap fraction (ATTBAR-MG5aMCNLO)
f	0.54 ± 0.03	0.50 ± 0.08	0.54 ± 0.03
χ^2_{min}/dof	29/20	11/17	40/38

global-recoil configuration, and predictions with the ATTBAR-MG5aMCNLO tune.

Although the global-recoil configuration is theoretically more consistent, the χ^2_{min} of the tuning for the local-recoil configuration is up to 17 points lower, and the agreement with the data is significantly better in the gap-fraction measurement, and in the 5th jet bin of the differential cross section as a function of jet multiplicity for jets with $p_{\text{T}} \geqslant 25$ GeV. The modeling of the first radiation includes fixed-order and all-order effects. For the current configuration of the MadGraph5_aMC@NLO+Pythia8 Monte Carlo generator it is not obvious which of these effects is responsible for the difference between the global and local recoil strategies.

8 Tune of the Powheg generator

The simultaneous ISR and FSR Pythia8 tune to the $t\bar{t}$ measurements, ATTBAR, is applied to the Powheg generator, with the exception of the $p^{\text{ISR}}_{\text{T,damp}}$ parameter, and the `hdamp` factor of Powheg is tuned to the $t\bar{t}$ data. The `hdamp` factor is parametrised as `hdamp` = $h \cdot m_t$, and the optimal value of h is obtained by tuning the Powheg+Pythia8 prediction to the differential $t\bar{t}$ cross sections as functions of jet multiplicity and jet transverse momentum, and to the gap fraction as a function of Q_0.

Table 15 shows the results of the tuning of the h parameter to the differential $t\bar{t}$ cross sections as functions of jet multiplicity and jet transverse momentum, and to the gap fraction as a function of Q_0, using the ATTBAR tune. The value of h obtained by tuning to the $t\bar{t}$ + jets measurements is consistent with the value obtained by tuning to the $t\bar{t}$ gap fraction, with the latter having larger uncertainty. The value of h, obtained by tuning to both measurements, is $h = 1.8^{+0.4}_{-0.3}$, which corresponds to `hdamp` $= 310^{+70}_{-50}$ GeV, and this tune is referred to as ATTBAR-POWHEG. Figure 10 shows the $t\bar{t}$ measurements compared to the Powheg+Pythia8 predictions with the Monash and ATTBAR-POWHEG tunes.

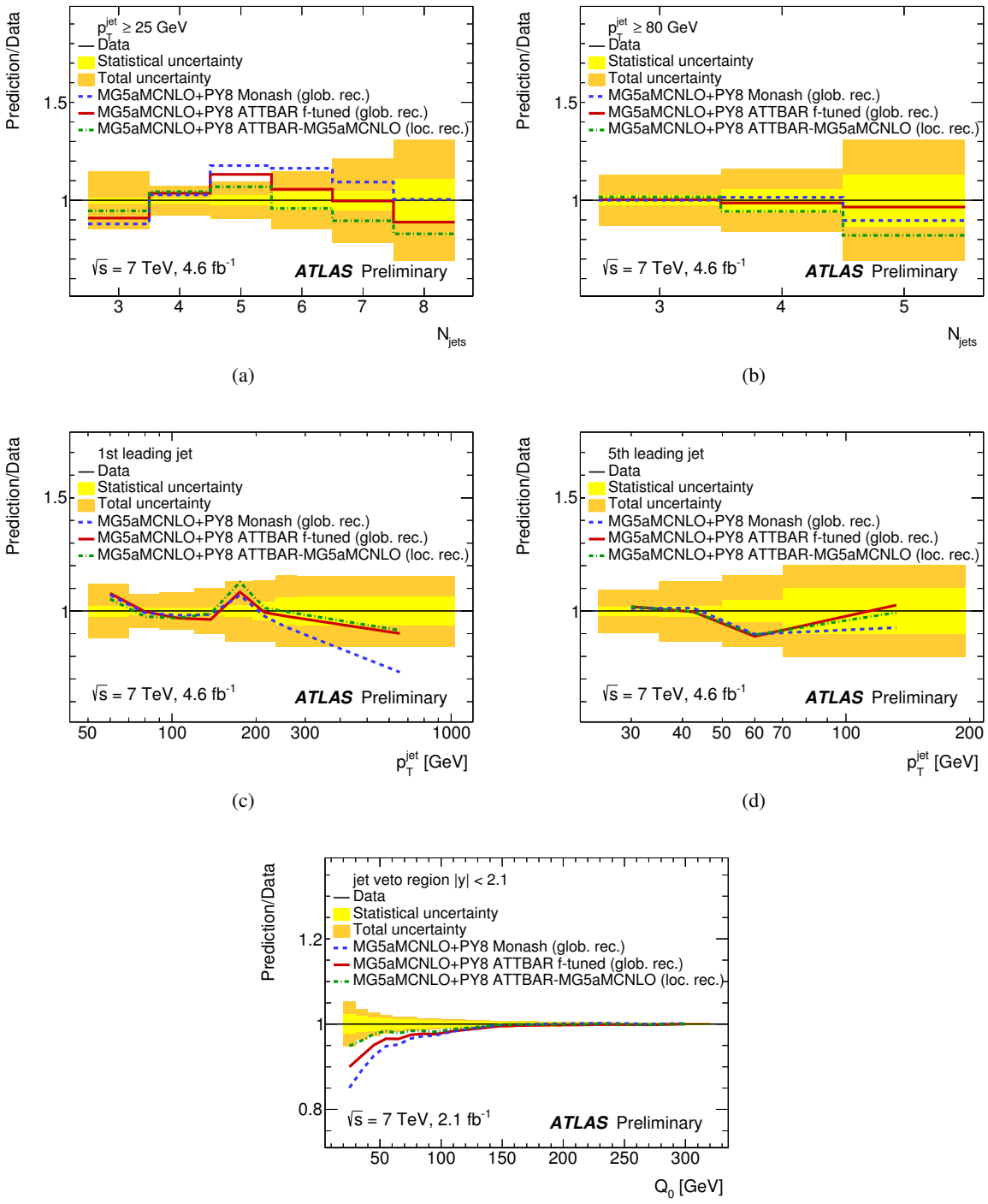

Figure 9: The MadGraph5_aMC@NLO+Pythia8 predictions with the Monash tune and the global-recoil configuration (blue dashed line), f-tuned predictions with the ATTBAR tune and the global-recoil configuration (red continuous line), and predictions with the ATTBAR-MG5aMCNLO tune (green dotted and dashed line), are compared to the measured differential $t\bar{t}$ cross sections as functions of (a) jet multiplicity for jets with $p_T^{jet} \geqslant 25$ GeV, (b) jet multiplicity for jets with $p_T^{jet} \geqslant 80$ GeV, (c) leading-jet transverse momentum, (d) 5th-leading jet transverse momentum, and (e) gap fraction as a function of Q_0. The relative statistical (yellow band) and total (orange band) experimental uncertainties are shown.

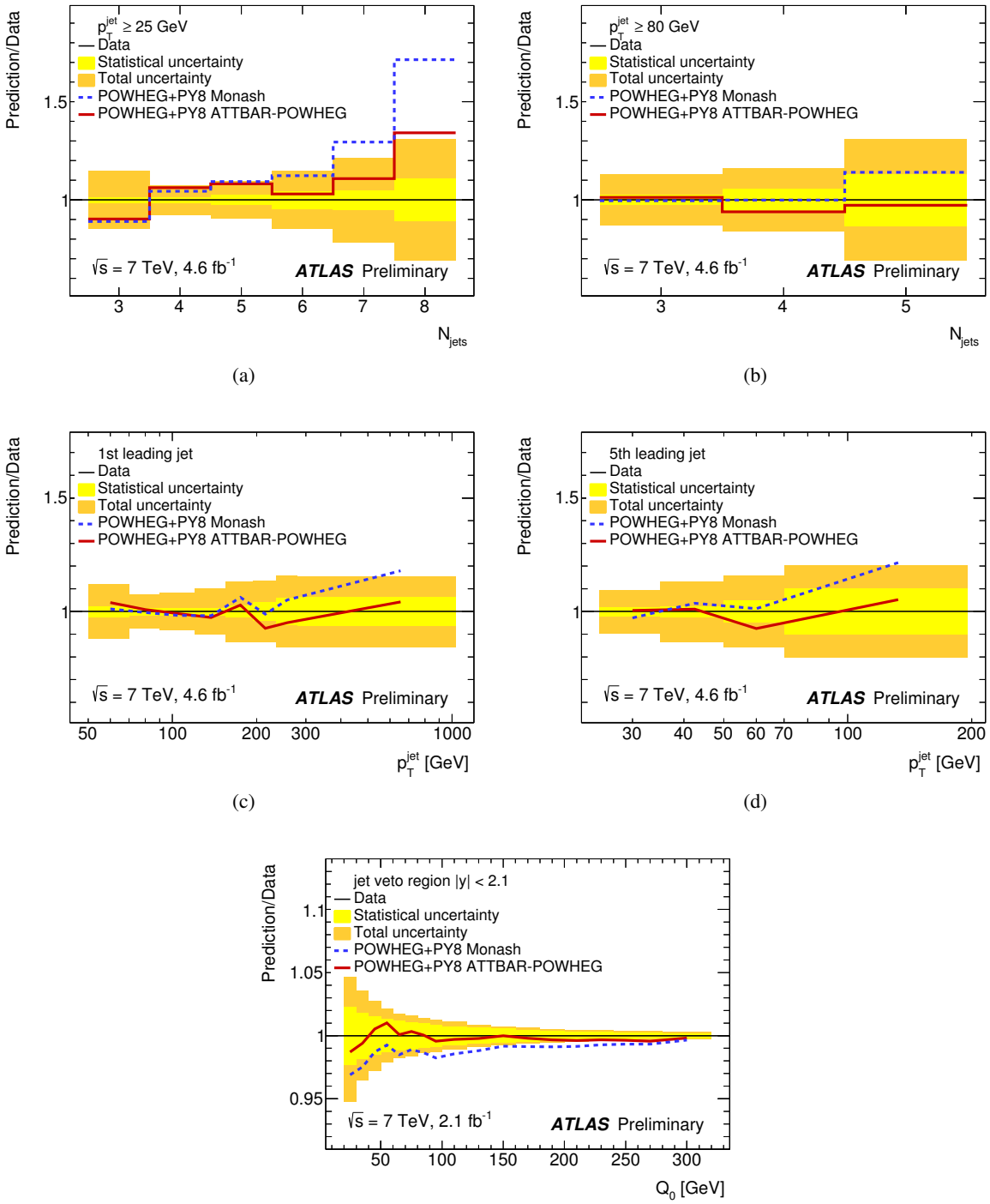

Figure 10: Predictions of POWHEG+PYTHIA8 with the ATTBAR-POWHEG (red continuous line) and Monash (blue dashed line) tunes compared to the measured differential $t\bar{t}$ cross sections as functions of (a) jet multiplicity for jets with $p_T^{jet} \geqslant 25$ GeV, (b) jet multiplicity for jets with $p_T^{jet} \geqslant 80$ GeV, (c) leading-jet transverse momentum, (d) 5th-leading jet transverse momentum, and (e) gap fraction as a function of Q_0. The relative statistical (yellow band) and total (orange band) experimental uncertainties are shown.

Table 15: Tuning results of the hdamp Powheg parameter to the differential $t\bar{t}$ cross sections as functions of jet multiplicity and jet transverse momentum ($t\bar{t}$+jets), and to the gap fraction as a function of Q_0 ($t\bar{t}$ gap fraction), using the ATTBAR tune.

Parameter	$t\bar{t}$+jets	$t\bar{t}$ gap fraction	$t\bar{t}$+jets and $t\bar{t}$ gap fraction (ATTBAR-POWHEG)
hdamp	$1.7^{+0.5}_{-0.3} \cdot m_t$	$2.2^{+2.9}_{-0.7} \cdot m_t$	$1.8^{+0.4}_{-0.3} \cdot m_t$
χ^2_{min}/dof	40/20	11.9/17	52.1/38

9 Summary and conclusions

Figures 11, 12, 13, and 14 show Pythia8 predictions with the ATTBAR tune, MadGraph5_aMC@NLO+Pythia8 predictions with the ATTBAR-MG5aMCNLO tune, and Powheg+Pythia8 predictions with the ATTBAR-POWHEG tune, compared to the ATLAS $t\bar{t}$ measurements. Table 16 summarises the settings of the ATTBAR tunes for the Pythia8, MadGraph5_aMC@NLO+Pythia8, and Powheg+Pythia8 generators.

Independent tunes of ISR and FSR parameters of the Pythia8 MC to the ATLAS $t\bar{t}$ measurements, and a simultaneous tune of the ISR and FSR parameters have been performed. The latter tune, named ATTBAR, is in very good agreement with the data. The value of $\alpha_s^{\text{ISR}}(m_Z)$ tuned to the $t\bar{t}$ data is in good agreement with previous tunes to the Z boson transverse momentum distribution measured by ATLAS [10], and the value of $\alpha_s^{\text{FSR}}(m_Z)$ is in good agreement with tunes to the LEP event shapes in Z boson hadronic decays [11–14]. The value of $p_{\text{T,min}}^{\text{FSR}}$ preferred by the tunes to the $t\bar{t}$ light-jet shapes is at the level of 1 GeV, which is significantly higher than the values used in the 4C and Monash tunes of about 0.5 GeV, and in disagreement with the determination of this parameter from LEP data [36]. Measurements of $t\bar{t}$ b-jet shapes are not well described by the Pythia8 MC, which predicts wider shapes than observed in the data. Significant disagreement with the data is observed in the region of $p_{\text{T}} \geqslant 70$ GeV and $r \geqslant 0.1$. Variations of the parameters considered in this study cannot account for the tension between the data and the predictions.

The ATTBAR tune is applied to the NLO+PS generators Powheg and MadGraph5_aMC@NLO, and the sensitivity of the $t\bar{t}$ measurements to additional parameters of these generators is studied. A reasonable agreement of the Powheg+Pythia8 predictions to the $t\bar{t}$ data is achieved by lowering the hdamp parameter, and the optimal value preferred by the data is $1.8 \cdot m_t$. The sensitivity of the $t\bar{t}$ data to the upper scale of the subtraction term, f = frac_low = frac_upp, of MadGraph5_aMC@NLO is studied. In order to match the subtraction term of MadGraph5_aMC@NLO, the Pythia8 FSR should be performed with a global recoil strategy. However, the MadGraph5_aMC@NLO+Pythia8 generator with the global recoil strategy for FSR predicts too high cross sections for $t\bar{t}$ + $\geqslant 5$ jets with $p_{\text{T}} \geqslant 25$ GeV, and too small gap fraction probabilities for a leading jet in the range $25 \leqslant p_{\text{T}} \leqslant 100$ GeV, as shown in Fig. 9. Such a disagreement is not observed when using the local recoil strategy for FSR.

The use of the uncertainties correlation in the tuning procedure gives a proper statistical meaning to the parameters values and their uncertainties, and provides a significant reduction of the parameters uncertainties.

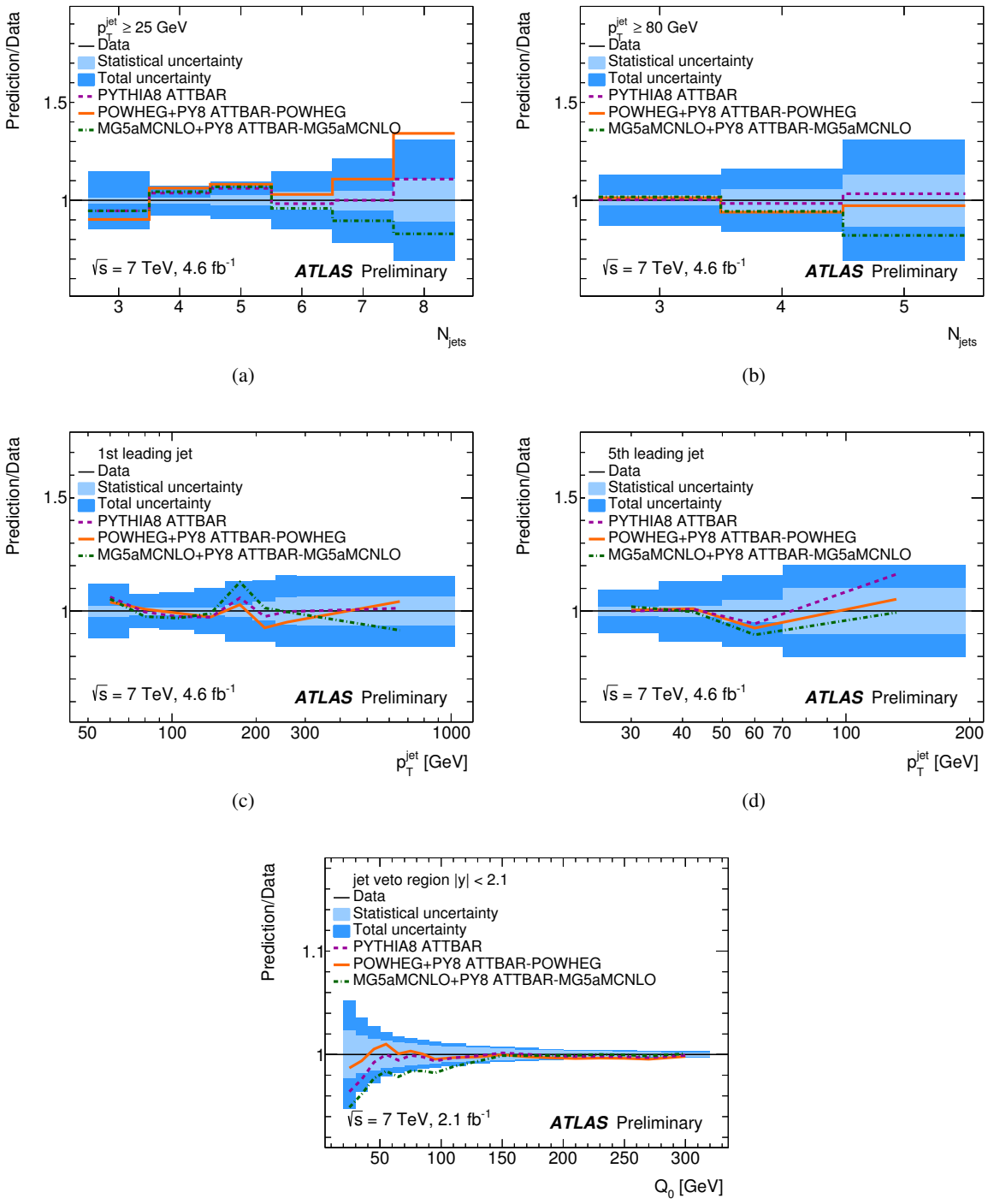

Figure 11: Predictions of Pythia8 (dashed magenta line), MadGraph5_aMC@NLO+Pythia8 (green dashed and dotted line), and Powheg+Pythia8 (orange continuous line) with the ATTBAR tunes compared to the measured differential $t\bar{t}$ cross sections as functions of (a) jet multiplicity for jets with $p_T^{jet} \geqslant 25$ GeV, (b) jet multiplicity for jets with $p_T^{jet} \geqslant 80$ GeV, (c) leading-jet transverse momentum, (d) 5th-leading jet transverse momentum, and (e) gap fraction as a function of Q_0. The relative statistical (light blue band) and total (dark blue band) experimental uncertainties are shown.

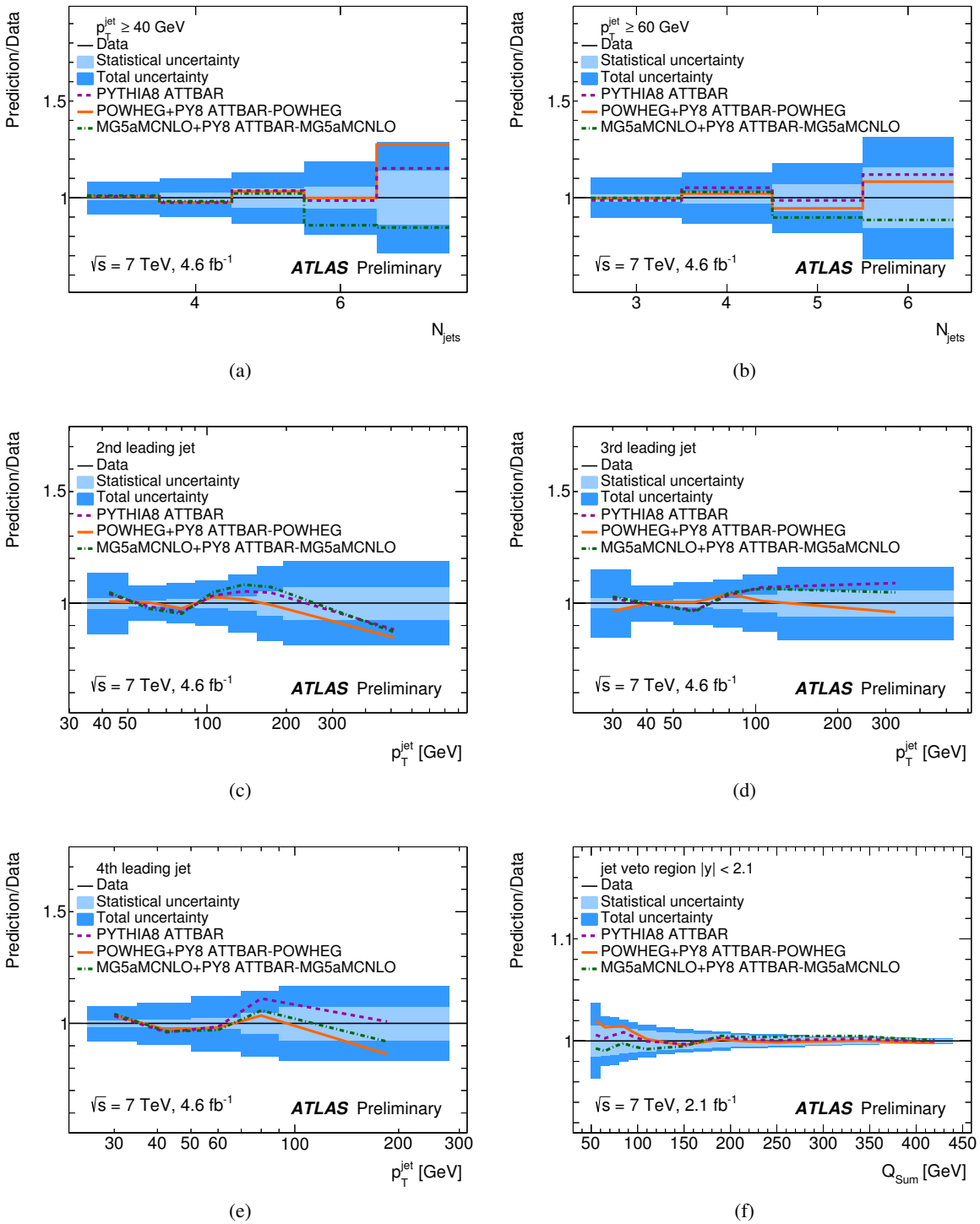

Figure 12: Predictions of Pythia8 (dashed magenta line), MadGraph5_aMC@NLO+Pythia8 (green dashed and dotted line), and Powheg+Pythia8 (orange continuous line) with the ATTBAR tunes compared to the measured differential $t\bar{t}$ cross sections as functions of (a) jet multiplicity for jets with $p_T{}^{jet} \geqslant 40$ GeV, (b) jet multiplicity for jets with $p_T{}^{jet} \geqslant 60$ GeV, (c) 2nd-leading-jet transverse momentum, (d) 3rd-leading-jet transverse momentum, (d) 4th-leading jet transverse momentum, and (e) gap fraction as a function of Q_{Sum}. The relative statistical (light blue band) and total (dark blue band) experimental uncertainties are shown.

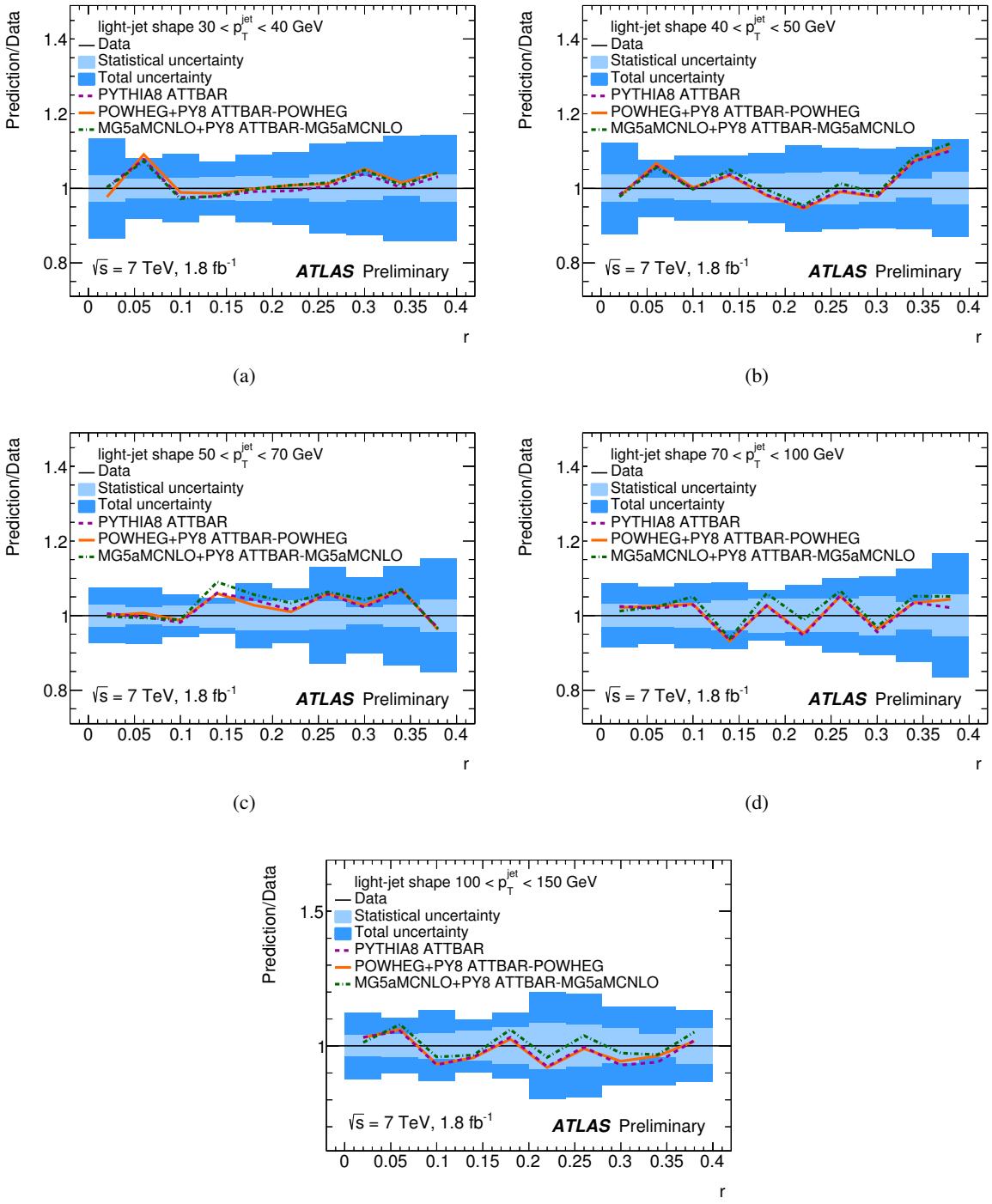

Figure 13: Predictions of PYTHIA8 (dashed magenta line), MadGraph5_aMC@NLO+PYTHIA8 (green dashed and dotted line), and POWHEG+PYTHIA8 (orange continuous line) with the ATTBAR tunes compared to the light-jet shapes as functions of the jet radius r for jets with (a) $30 < p_{\mathrm{T}}^{\mathrm{jet}} < 40$, (b) $40 < p_{\mathrm{T}}^{\mathrm{jet}} < 50$, (c) $50 < p_{\mathrm{T}}^{\mathrm{jet}} < 70$, (d) $70 < p_{\mathrm{T}}^{\mathrm{jet}} < 100$, and (e) $100 < p_{\mathrm{T}}^{\mathrm{jet}} < 150$. The relative statistical (light blue band) and total (dark blue band) experimental uncertainties are shown.

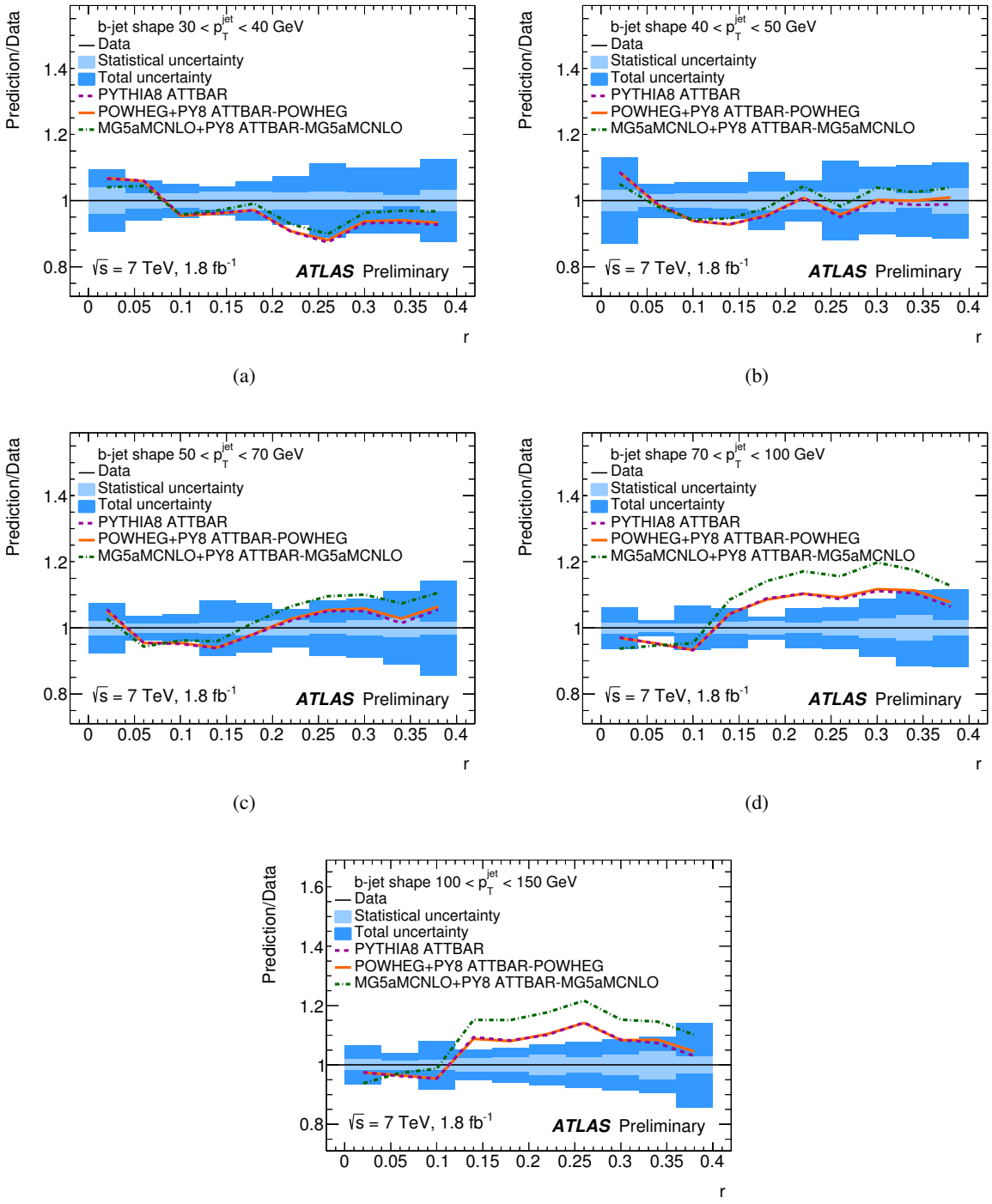

Figure 14: Predictions of PYTHIA8 (dashed magenta line), MadGraph5_aMC@NLO+PYTHIA8 (green dashed and dotted line), and POWHEG+PYTHIA8 (orange continuous line) with the ATTBAR tunes compared to the *b*-jet shapes as functions of the jet radius r for jets with (a) $30 < p_{\mathrm{T}}^{\mathrm{jet}} < 40$, (b) $40 < p_{\mathrm{T}}^{\mathrm{jet}} < 50$, (c) $50 < p_{\mathrm{T}}^{\mathrm{jet}} < 70$, (d) $70 < p_{\mathrm{T}}^{\mathrm{jet}} < 100$, and (e) $100 < p_{\mathrm{T}}^{\mathrm{jet}} < 150$. The relative statistical (light blue band) and total (dark blue band) experimental uncertainties are shown.

Table 16: Options and parameters settings of the ATTBAR, ATTBAR-MG5aMCNLO and ATTBAR-POWHEG tunes of PYTHIA8, MADGRAPH5_AMC@NLO+PYTHIA8, and POWHEG+PYTHIA8. All the other parameters and model switches correspond to the settings of the base tune (Monash) for PYTHIA8, and to the default values for MadGraph5_aMC@NLO and POWHEG. The '-' symbol is used in case the setting is not applicable.

PYTHIA8 settings	ATTBAR	ATTBAR-MG5aMCNLO	ATTBAR-POWHEG
SpaceShower:alphaSvalue	0.121	0.121	0.121
SpaceShower:pTdampMatch	1	0	0
SpaceShower:pTdampFudge	1.18	-	-
TimeShower:alphaSvalue	0.137	0.137	0.137
TimeShower:pTmin	1.26	1.26	1.26
MultipartonInteractions:pT0Ref	2.16	2.16	2.16
TimeShower:globalRecoil	-	off	-
SpaceShower:pTmaxMatch	0	1	2
SpaceShower:MEcorrections	on	off	on
TimeShower:MEcorrections	on	off	on
POWHEG:veto	-	-	1
POWHEG:vetoCount	-	-	3
POWHEG:pThard	-	-	0
POWHEG:pTemt	-	-	0
POWHEG:emitted	-	-	0
POWHEG:pTdef	-	-	2
POWHEG:MPIveto	-	-	0
MADGRAPH5_AMC@NLO settings			
frac_upp	-	0.54	-
frac_low	-	0.54	-
scaleMCdelta	-	0	-
POWHEG settings			
hdamp	-	-	$1.8 \cdot m_t$

Acknowledgements

We thank Torbjörn Sjöstrand and Stefan Prestel for fruitful discussions on this subject.

References

[1] J. M. Katzy, *QCD Monte-Carlo model tunes for the LHC*, Prog. Part. Nucl. Phys. **73** (2013) 141–187.

[2] P. Skands, S. Carrazza and J. Rojo, *Tuning PYTHIA 8.1: the Monash 2013 Tune*, Eur. Phys. J. C **74** (2014) 3024, arXiv: 1404.5630 [hep-ph].

[3] H. Schulz and P. Skands, *Energy Scaling of Minimum-Bias Tunes*, Eur. Phys. J. C **71** (2011) 1644, arXiv: 1103.3649 [hep-ph].

[4] ATLAS Collaboration, *Measurement of $t\bar{t}$ production with a veto on additional central jet activity in pp collisions at $\sqrt{s}$ = 7 TeV using the ATLAS detector*, Eur. Phys. J. C **72** (2012) 2043, arXiv: 1203.5015 [hep-ex].

[5] ATLAS Collaboration, *Measurement of jet shapes in top-quark pair events at $\sqrt{s}$ = 7 TeV using the ATLAS detector*, Eur. Phys. J. C **73** (2013) 2676, arXiv: 1307.5749 [hep-ex].

[6] ATLAS Collaboration, *Measurement of the $t\bar{t}$ production cross-section as a function of jet multiplicity and jet transverse momentum in 7 TeV proton–proton collisions with the ATLAS detector*, JHEP **1501** (2015) 020, arXiv: 1407.0891 [hep-ex].

[7] ATLAS Collaboration, *Differential top-antitop cross-section measurements as a function of observables constructed from final-state particles using pp collisions at $\sqrt{s}$ = 7 TeV in the ATLAS detector* (2015), arXiv: 1502.05923 [hep-ex].

[8] ATLAS Collaboration, *ATLAS Pythia 8 tunes to 7 TeV data*, ATL-PHYS-PUB-2014-021, 2014, URL: https://atlas.web.cern.ch/Atlas/GROUPS/PHYSICS/PUBNOTES/ATL-PHYS-PUB-2014-021/.

[9] T. Sjöstrand et al., *An Introduction to PYTHIA 8.2* (2014), arXiv: 1410.3012 [hep-ph].

[10] ATLAS Collaboration, *Measurement of the Z/γ^* boson transverse momentum distribution in pp collisions at $\sqrt{s}$ = 7 TeV with the ATLAS detector*, JHEP **1409** (2014) 145, arXiv: 1406.3660 [hep-ex].

[11] P. Achard et al., *Studies of hadronic event structure in e^+e^- annihilation from 30-GeV to 209-GeV with the L3 detector*, Phys. Rept. **399** (2004) 71–174, arXiv: hep-ex/0406049 [hep-ex].

[12] R. Barate et al., *Studies of quantum chromodynamics with the ALEPH detector*, Phys. Rept. **294** (1998) 1–165.

[13] P. Abreu et al., *Tuning and test of fragmentation models based on identified particles and precision event shape data*, Z. Phys. **C73** (1996) 11–60.

[14] P. Pfeifenschneider et al., *QCD analyses and determinations of alpha(s) in e+ e- annihilation at energies between 35-GeV and 189-GeV*, Eur. Phys. J. C **17** (2000) 19–51, arXiv: hep-ex/0001055 [hep-ex].

[15] V. M. Abazov et al., *Precision measurement of the top-quark mass in lepton+jets final states*, Phys. Rev. Lett. **113** (2014) 032002, arXiv: 1405.1756 [hep-ex].

[16] V. M. Abazov et al., *Precision measurement of the top-quark mass in lepton+jets final states* (2015), arXiv: 1501.07912 [hep-ex].

[17] V. M. Abazov et al., *Precise study of the Z/γ^* boson transverse momentum distribution in $p\bar{p}$ collisions using a novel technique*, Phys. Rev. Lett. **106** (2011) 122001, arXiv: 1010.0262 [hep-ex].

[18] T. Aaltonen et al., *Top quark mass measurement using the template method at CDF*, Phys. Rev. D **83** (2011) 111101, arXiv: 1105.0192 [hep-ex].

[19] P. Nason, *A New method for combining NLO QCD with shower Monte Carlo algorithms*, JHEP **0411** (2004) 040, arXiv: hep-ph/0409146 [hep-ph].

[20] S. Alioli et al., *A general framework for implementing NLO calculations in shower Monte Carlo programs: the POWHEG BOX*, JHEP **1006** (2010) 043, arXiv: 1002.2581 [hep-ph].

[21] S. Frixione, P. Nason and C. Oleari, *Matching NLO QCD computations with Parton Shower simulations: the POWHEG method*, JHEP **0711** (2007) 070, arXiv: 0709.2092 [hep-ph].

[22] J. Alwall et al., *The automated computation of tree-level and next-to-leading order differential cross sections, and their matching to parton shower simulations*, JHEP **1407** (2014) 079, arXiv: 1405.0301 [hep-ph].

[23] R. Corke and T. Sjöstrand, *Interleaved Parton Showers and Tuning Prospects*, JHEP **1103** (2011) 032, arXiv: 1011.1759 [hep-ph].

[24] J. Pumplin et al., *New generation of parton distributions with uncertainties from global QCD analysis*, JHEP **0207** (2002) 012, arXiv: hep-ph/0201195 [hep-ph].

[25] R. D. Ball et al., *Parton distributions with LHC data*, Nucl. Phys. B **867** (2013) 244–289, arXiv: 1207.1303 [hep-ph].

[26] R. Corke and T. Sjöstrand, *Improved Parton Showers at Large Transverse Momenta*, Eur. Phys. J. C **69** (2010) 1–18, arXiv: 1003.2384 [hep-ph].

[27] T. Sjöstrand and P. Z. Skands, *Transverse-momentum-ordered showers and interleaved multiple interactions*, Eur. Phys. J. C **39** (2005) 129–154, arXiv: hep-ph/0408302 [hep-ph].

[28] S. Frixione et al., *A Positive-weight next-to-leading-order Monte Carlo for heavy flavour hadroproduction*, JHEP **0709** (2007) 126, arXiv: 0707.3088 [hep-ph].

[29] H.-L. Lai et al., *New parton distributions for collider physics*, Phys. Rev. D **82** (2010) 074024, arXiv: 1007.2241 [hep-ph].

[30] S. Alioli et al., *NLO Higgs boson production via gluon fusion matched with shower in POWHEG*, JHEP **0904** (2009) 002, arXiv: 0812.0578 [hep-ph].

[31] ATLAS Collaboration, *Comparison of Monte Carlo generator predictions for gap fraction and jet multiplicity observables in $t\bar{t}$ events*, ATL-PHYS-PUB-2014-005, 2014, URL: https://atlas.web.cern.ch/Atlas/GROUPS/PHYSICS/PUBNOTES/ATL-PHYS-PUB-2014-005.

[32] ATLAS Collaboration, *Comparison of Monte Carlo generator predictions to ATLAS measurements of top pair production at 7 TeV*, ATL-PHYS-PUB-2015-002, 2015, URL: http://atlas.web.cern.ch/Atlas/GROUPS/PHYSICS/PUBNOTES/ATL-PHYS-PUB-2015-002/.

[33] A. Buckley et al., *Systematic event generator tuning for the LHC*, Eur. Phys. J. C **65** (2010) 331–357, arXiv: 0907.2973 [hep-ph].

[34] A. Buckley et al., *Rivet user manual*, Comput. Phys. Commun. **184** (2013) 2803–2819, arXiv: 1003.0694 [hep-ph].

[35] F. James and M. Roos, *Minuit: A System for Function Minimization and Analysis of the Parameter Errors and Correlations*, Comput. Phys. Commun. **10** (1975) 343–367.

[36] N. Fischer et al., *Revisiting radiation patterns in e^+e^- collisions*, Eur. Phys. J. C **74**.4 (2014) 2831, arXiv: 1402.3186 [hep-ph].

[37] S. Argyropoulos and T. Sjöstrand, *Effects of color reconnection on $t\bar{t}$ final states at the LHC*, JHEP **1411** (2014) 043, arXiv: 1407.6653 [hep-ph].

[38] J. M. Campbell et al., *Top-pair production and decay at NLO matched with parton showers* (2014), arXiv: 1412.1828 [hep-ph].

[39] CMS Collaboration, *Study of the underlying event, b-quark fragmentation and hadronization properties in tbart events*, CMS-PAS-TOP-13-007, 2012, URL: https://cds.cern.ch/record/1600599.

[40] ATLAS Collaboration, *Measurement of distributions sensitive to the underlying event in inclusive Z-boson production in pp collisions at $\sqrt{s} = 7$ TeV with the ATLAS detector*, Eur. Phys. J. C **74** (2014) 3195, arXiv: 1409.3433 [hep-ex].